EXPERIMENTAL STUDY OF CO_2 INJECTION INTO CARBONATE DEPLETED FIELD: A CASE STUDY FROM CENTRAL LUCONIA FIELD, SARAWAK, EAST MALAYSIA

NUR ZAFIRAH BINTI MAT RAZALI

FACULTY OF SCIENCE
UNIVERSITI MALAYA
KUALA LUMPUR

2021

EXPERIMENTAL STUDY OF CO$_2$ INJECTION INTO CARBONATE DEPLETED FIELD: A CASE STUDY FROM CENTRAL LUCONIA FIELD, SARAWAK, EAST MALAYSIA

NUR ZAFIRAH BINTI MAT RAZALI

DISSERTATION SUBMITTED IN FULFILMENT OF THE REQUIREMENTS FOR THE DEGREE OF MASTER OF SCIENCE

DEPARTMENT OF GEOLOGY
FACULTY OF SCIENCE
UNIVERSITI MALAYA
KUALA LUMPUR

2021

<div align="center">

UNIVERSITI MALAYA

ORIGINAL LITERARY WORK DECLARATION

</div>

Name of Candidate: **NUR ZAFIRAH BINTI MAT RAZALI**

atric No: **17006472 / SMA170006**

Name of Degree: **MASTER OF SCIENCE**

Title of Dissertation ("this work"):

EXPERIMENTAL STUDY OF CO_2 INJECTION INTO CARBONATE DEPLETED FIELD: A CASE STUDY FROM CENTRAL LUCONIA FIELD, SARAWAK, EAST MALAYSIA

Field of Study: **GEOLOGY**

I do solemnly and sincerely declare that:

(1) I am the sole author/writer of this Work;

(2) This Work is original;

(3) Any use of any work in which copyright exists was done by way of fair dealing and for permitted purposes and any excerpt or extract from, or reference to or reproduction of any copyright work has been disclosed expressly and sufficiently and the title of the Work and its authorship have been acknowledged in this Work;

(4) I do not have any actual knowledge nor do I ought reasonably to know that the making of this work constitutes an infringement of any copyright work;

(5) I hereby assign all and every rights in the copyright to this Work to the University of Malaya ("UM"), who henceforth shall be owner of the copyright in this Work and that any reproduction or use in any form or by any means whatsoever is prohibited without the written consent of UM having been first had and obtained;

(6) I am fully aware that if in the course of making this Work I have infringed any copyright whether intentionally or otherwise, I may be subject to legal action or any other action as may be determined by UM.

Candidate's Signature   Date: 12 January 2021

Subscribed and solemnly declared before,

Witness's Signature   Date: 12 January 2021

Name:

Designation:

EXPERIMENTAL STUDY OF CO2 INJECTION INTO CARBONATE DEPLETED FIELD: A CASE STUDY FROM CENTRAL LUCONIA FIELD, SARAWAK, EAST MALAYSIA

ABSTRACT

This study aimed to address the challenges and strategies to determine the critical rate of CO_2 injection into carbonate depleted gas fields. In this research, the critical rate is the maximum allowable injection rate before formation damage initiation. The cause of formation damage could be due to in-situ mobilization or trapping of migratory fines resulting in plugging of the flow path. This study performed a thorough investigation of a different rock-fluid system to evaluate the safe injection limit, as the critical rate is different for each rock-fluid system. The geochemical effect of CO_2 injection toward carbonate formation was also investigated in this research. Other than that, the porosity and permeability changes due to CO_2-brine-rock multiphase flow characteristics were considered to understand the feasibility of CO_2 sequestration into carbonate formation. This research discussed experimental design to mimic the injection scenario of CO_2 into carbonate depleted gas field. Therefore, several sets of core flooding experiments were conducted under reservoir conditions using representative native cores, CO_2, and synthetic formation brine. Abrupt changes in differential pressure (ΔP), analysis of effluent collected after CO_2 multi-rate flow, and pH reading are the key indicators to consider that the condition has reached a critical rate. The experimental result demonstrated the existence of fines migration, scale formation, and salt precipitation after the core was subjected to supercritical CO_2 multi-rate flow. Considering these issues and challenges associated with injectivity, this study recommended a maximum injection rate prior to field scale injection.

Keywords: core flooding, carbonate, CO_2 injection, dissolution, precipitation.

KAJIAN MENGENAI SUNTIKAN CO$_2$ KE DALAM LAPANGAN KARBONATE YANG SUDAH DIPENUHI AIR. KAJIAN DARIPADA CENTRAL LUCONIA

ABSTRAK

Tujuan kajian ini adalah untuk mengenal pasti cabaran yang dihadapi dan menyediakan strategi untuk menentukan kadar kritikal suntikan CO$_2$ ke dalam lapangan karbonat yang sudah dipenuhi air. Kadar kritikal bermaksud kadar suntikan maksimum yang dibenarkan sebelum permulaan kerosakan batu karbonat. Punca kerosakan batu karbonat berkemungkinan disebabkan oleh pergerakan komponen batu batu kecil yang disebabkan oleh kelajuan CO$_2$ yang dikenakan terhadap batu atau disebabkan batu batu kecil menutupi rongga palam teras lalu mengganggu pergerakan CO$_2$ untuk mengalir. Kajian ini memberikan fokus menyeluruh terhadap setiap sistem bendalir batuan yang unik untuk menilai batas suntikan yang selamat, kerana kadar kritikal adalah berbeza untuk setiap sistem cairan batuan. Oleh yang demikian, untuk menganalisis keadaan ini, satu set eksperimen banjir palam teras dijalankan menggunakan keadaan asal palam teras iaitu palam teras daripada lapangan karbonat, CO$_2$ dan air garam. Perubahan yang mendadak terhadap tekanan (ΔP), analisis efluen yang dikumpulkan selepas aliran berbilang kadar CO$_2$ dan bacaan pH adalah penunjuk utama untuk mempertimbangkan bahawa keadaan telah mencapai kadar kritikal. Keputusan eksperimen menunjukkan adanya penghijrahan batu batu kecil, pembentukan skala dan pemendapan garam selepas terasnya mengalami aliran CO$_2$ berbilang kadar selama lebih kurang dua minggu. Dengan mempertimbangkan isu dan cabaran yang dikaitkan dengan suntikan, kajian ini mencadangkan kadar suntikan maksimum sebelum suntikan skala medan dijalankan.

Kata Kunci: banjir palam teras, karbonat, suntikan CO$_2$, larutan dan pemendakan

ACKNOWLEDGEMENTS

TABLE OF CONTENTS

LIST OF FIGURES

LIST OF TABLES

LIST OF SYMBOLS AND ABBREVIATIONS

atm	:	atmospheric
ΔP	:	differential pressure
g/cc	:	gram per cubic centimeter
mD	:	millidarcy
ml/min	:	millimeter per minute
Psi	:	pound per square inch
Psig	:	pounds per square inch gauge
Kw	:	water permeability
WAG	:	Water Alternating Gas

CHAPTER 1: INTRODUCTION

1.1 Background and Problem Description

The first part of this chapter focuses on the effect of greenhouse gasses due to the high level of atmospheric CO_2 and mitigation to encounter this issue by introducing carbon capture and storage (CCS) technology. The second part discusses the research objectives, and the chapter ends with a brief overview of the paper published based on the contents of this dissertation.

1.1.1 Global Warming

Human influence on the climate system is evident and undeniable. The release of greenhouse gasses such as carbon dioxide (CO_2), methane (CH_4), nitrous oxide (N_2O), and fluorinated gases (F-gases) have taken a toll on the earth's surface. The emission of CO_2 produced by human activities comes from the combustion of fossil fuels, coal, oil, and natural gas. Other than that, CO_2 is also spread from social activities such as deforestation, agriculture, and degradation of soil. Meanwhile, CH_4 and N_2O are produced by direct human-induced impacts from agriculture activities, energy consumption, and the effect of biomass burning on the atmosphere. As for F-gases, this type of gas generally formed from industrial processes, refrigeration, and consumer product, which include hydrofluorocarbons, perfluorocarbons, and sulfur hexafluoride.

The greenhouse gasses act as a thermal blanket for the earth, absorbing heat from the sun and keeping its surface warm to support life. CO_2 emits radiant energy within the thermal infrared range that induced temperature elevation if the excess CO_2 is not managed correctly. As the CO_2 concentration increases, the earth's atmosphere and surface are gradually heated up because of the trapped thermal infrared radiation fails to

escape into outer space. This is due to the increasing levels of greenhouse gasses forming a thick blanket.

Since the beginning of the industrial revolution in 1750, CO_2 emission has caused severe weather perturbation and contributed to globally rising temperatures that lead to climate change (Herzog, 2001; Chu, 2009; Saeedi & Rezaee, 2012). It has been predicted that if CO_2 emissions remain as it is, this condition will cause harmful effects on ecosystems, biodiversity and the live hoods of people worldwide (Mora et al., 2013).
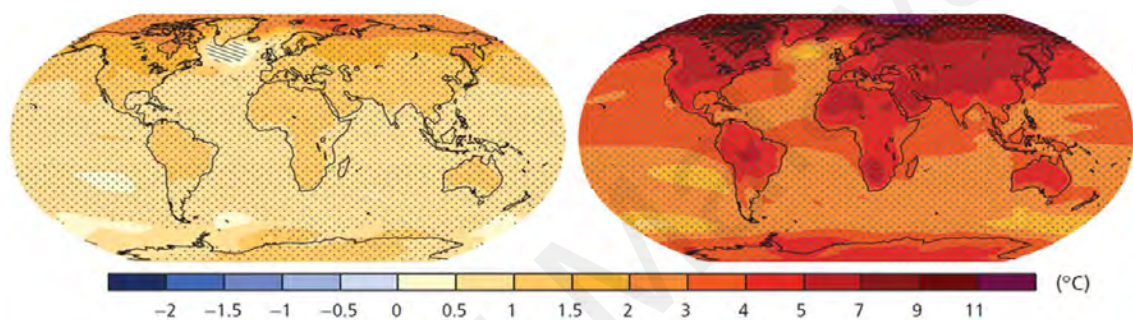
Figure 1.1: Change in average surface temperature (1986−2005 to 2081−2100) (Pachauri et al., 2014).

Eventually, these phenomena will cause extreme weather and climate events, including but not limited to a decrease in cold temperature extremes, an increase in warm temperature extremes, and an increase in extreme high sea levels (Pachauri et al., 2014). CO_2 is the most significant since it exists in the largest concentration (76%) and has a longer lifetime than CH_4. Recently, a continuous increase in CO_2 emission has contributed to the discharge of chlorofluorocarbons (CFCs). CFCs potentially trapped the head a thousand times greater than CO_2 and degrade the earth's ozone layer.

1.1.2 Carbon Capture and Storage (CCS) Project

To address these alarming issues, relatively new technology is developed to sequester CO2 and subsequently to store them in secure locations. This project is called carbon capture and storage projects at which CO_2 from industrial sources is captured,

transported, and injected into the underground for permanent storage (Global, 2015). Captured CO_2 is separated from other gases generated at factories such as coal, natural gas power plants, and hydrocarbon refineries prior to transportation to a suitable site for geological storage. Transportation of CO_2 is typically using pipelines and ships, sometimes trucks or trains for a small amount of CO_2. Thenceforth, CO_2 is injected into underground rock formations.

Figure 1.2: Large scale CCS projects (Global, 2015).

Ideally, there are four key elements significant for CO_2 storage, namely depth, location, containment, and capacity. The storage site needs to be more than 1 km from the earth's surface and must be permeable for the CO_2 to move through the rock and get trapped in the pores. Other than that, injected CO_2 is preferred to be in a supercritical state at which it has properties of both a gas and a liquid (Zhang & Song, 2014). Under these conditions, CO_2 possesses the solvating power of a liquid and the diffusivity of gas hence lead to higher CO_2 volume for sequestration.

To achieve these circumstances, CO_2's temperature must be ≥ 30.98 ℃ with pressure ≥ 1070 psi (Pham et al., 2016; Wang et al., 2018). CO_2 needs to be contained in a layer of dense, impenetrable rock above it known as caprock, to prevent CO_2 movement

upward. Besides, the sequestration sites require sufficient storage capacity to hold the amount of CO_2 planned to be injected over the life of a project.
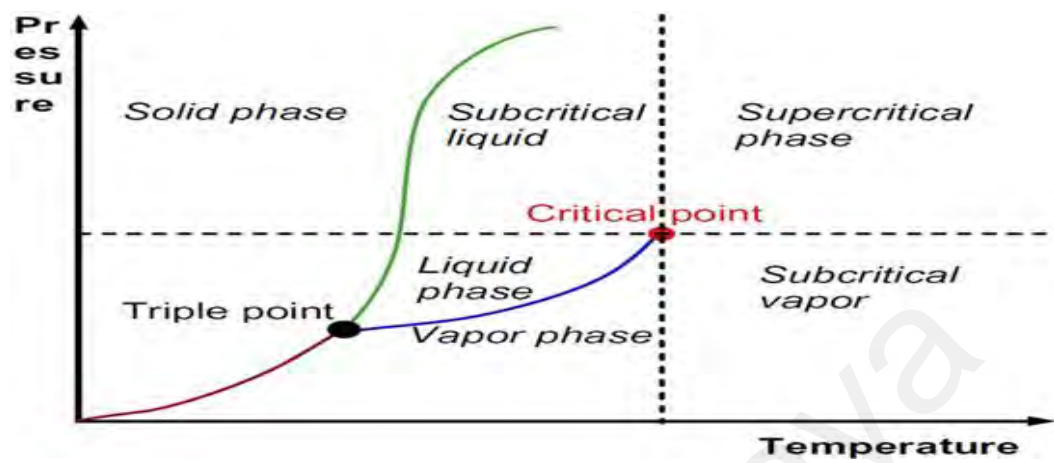
Figure 1.3: The pressure vs. temperature diagram (Pham et al., 2016).

1.1.3   Geological Storage

There are several potential geological CO_2 storage sites. Geological storage of CO_2 can be undertaken in a variety of geological settings such as basins, oil fields, depleted gas fields, deep coal seams and saline aquifer (Bachu, 2003; Rubin, 2005; Polak et al., 2011; Akintunde et al., 2013; Song & Zhang, 2013). It was mentioned that saline aquifers have the highest storage capacity among all other types of underground storage reservoirs (Mohamed, et al., 2011).
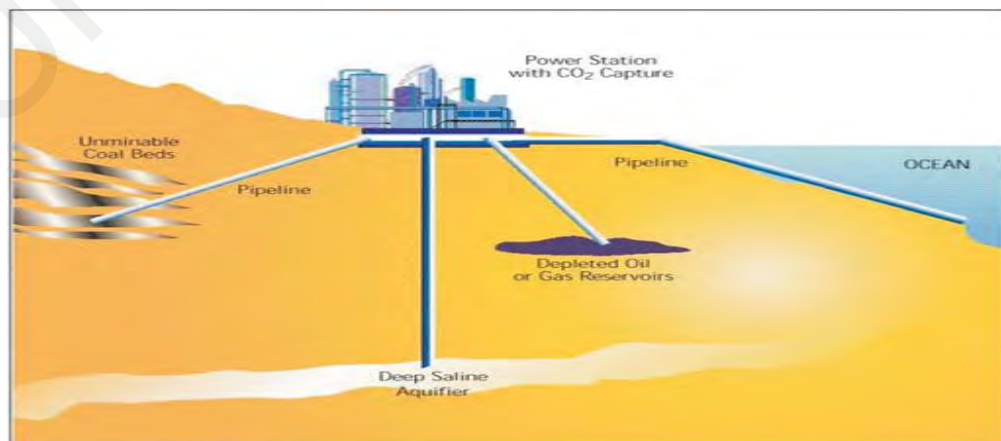
Figure 1.4: Geological storage location (Davison et al., 2001).

1.1.3.1 Depleted Oil and Gas Reservoir

This storage location is where thousands of oil and gas fields are approaching the ends of their economically productive lives due to intensive petroleum exploitation. The attractive feature for depleted oil and gas reservoirs as a CO_2 sequestration site would be a proven geological structure of porous rocks with impermeable cap rock, traps, and known to have held hydrocarbon for millions of years. Therefore, these fields could be adapted easily for storage of CO_2. Other than small exploration costs, there is potential to re-apply existing equipment for transportation and CO_2 injection.

Nevertheless, it was mentioned by Davison et al. (2001) that there would need to be some changes in current practice to make use of depleted oil and gas reservoirs for CO_2 storage.

1.1.3.2 Deep Saline Reservoirs

A saline aquifer refers to sedimentary rock types saturated with saline water and unsuitable for supplying potable water. The aquifers that would be used for CO_2 storage must be deep underground, and the technique of CO_2 injection for this reservoir is similar to those for depleted fields.

While not as nearly as common as injecting CO_2 for EOR, this storage location is being practiced in Sleipner, Norway, North Sea. It was started in 1996 when the CO_2 is directly injected into the deep saline aquifer of 1 km deep under the seabed in the Utsira sand formation. Located in the North Sea at about 200 km off the Norwegian coast, the natural gas field mainly made of methane, which contains 4-10% of CO_2. Another case study for CO_2 storage in the deep saline aquifer is located in the natural gas field in Salah (Algeria), which is estimated to hold a storage capacity of 17 million tons of CO_2.

1.1.3.3 Coal-bed Methane

In this case, injected CO_2 binds to the coal and is sequestered permanently. The CO_2 is injected into coalbeds to exchange with methane. However, this storage location is in the research phase, with no operational projects.

1.1.4 Trapping Mechanism

Theoretically, injected CO_2 will be stored by different types of trapping mechanisms such as hydrodynamic/structural/stratigraphic trapping, residual or capillary trapping, solubility trapping, and mineral trapping.
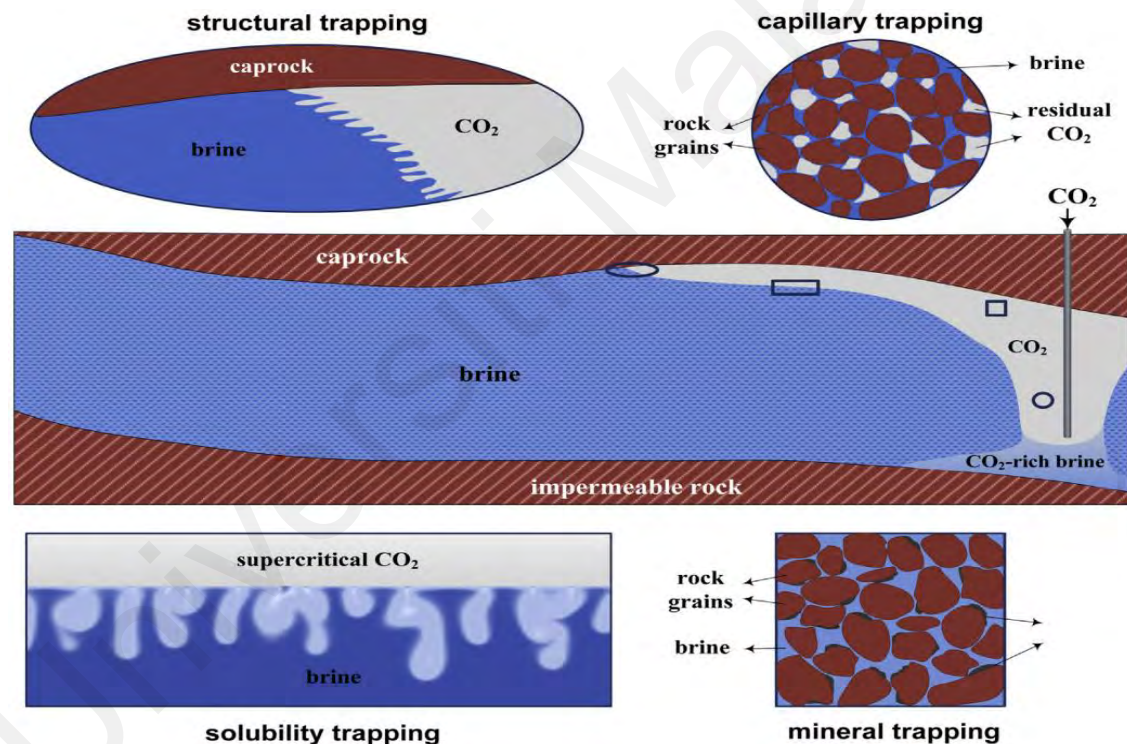
Figure 1.5: Schematic illustration of fluid dynamics and trapping mechanisms associated with geo-sequestration of CO_2 in saline aquifers, including structural trapping, and capillary trapping, solubility trapping, and mineral trapping (Emami-Meybodi et al., 2015).

1.1.4.1 Hydrodynamic/Structural/Stratigraphic Trapping

This trapping mechanism refers to supercritical CO_2 trapped under low permeability caprock. The density of supercritical CO_2 being less than water tended to rise buoyantly

6

until it reaches the caprock. This is also known as viscous fingering. Since the caprock has a capillary entry pressure greater than the buoyancy force, supercritical CO_2 will accumulate in such a structural and stratigraphic feature. Typically, this trapping mechanism may take effect after 20 – 40 years of injection period depending on rock type.

The trapping efficiency is determined by the structure of the sedimentary basins, which have an intricate plumbing system by the location of high and low permeability strata that control the flow of fluids through the basin (Zhang & Song, 2014). Anticlinal folds or seal fault block is the most common structural traps that are mostly found in reservoirs that have held oil and gas for millions of years.

Injected CO_2 may take millions of years to travel by buoyancy forces up-dip to reach the surface before it leaks back into the atmosphere. This trapping mechanism highly depends on the sealing capacity of caprock, making it a big challenge for site selection (Song & Zhang, 2013; Zhang & Song, 2014).

1.1.4.2 Residual/Capillary Trapping

As the supercritical CO_2 is injected into the formations, it first displaces brine in a co-current fashion until the injection is stopped. Then, CO_2 will migrate up towards, and brines flows downwards due to density differences and replace CO_2 as a wetting phase. Thus, CO_2 trapped in a small cluster of pores while being saturated by brine. The capillary forces and relative permeability effects will contribute to converting the CO_2 injected into an immobile phase. This is the same concept on how the hydrocarbon was held for millions of years. Typically, this trapping mechanism may take effect hundreds of years post-injection depending on rock type.

1.1.4.3   Solubility Trapping

Solubility trapping is where CO_2 dissolves in brine, just like sugar dissolves in tea. Dissolved CO_2 in brine is denser than brine; thus will sink to the bottom of formation over time, trapping the CO_2 even more securely. The dissolution would increase the density of brine up to approximately 1% compared with the original brine (Zhang & Song, 2014). Typically, this trapping mechanism may take effect hundreds of years post-injection depending on rock type.

1.1.4.4   Mineral Trapping

Mineral trapping refers to dissolve CO_2 from the solubility trapping mechanism change into a stable mineral phase via reactions with mineral and organic matter in the formation. For example, the creation of carbonates as a result of aluminosilicate minerals can be an essential trapping mechanism though the timeline is on the order of 100's to 1000's of years (Xu et al., 2005).

1.1.5   Salt Precipitation

Injection of CO_2 into saline aquifers will cause carbonation of contacted in situ brines, disturbing the chemical equilibrium that was established over geological time frames between the brine and host rock (Jin et al., 2016). As NaCl is the most abundant compound in a saline aquifer, saline formation water will be evaporated when CO_2 is injected into the formation, which gives rise to salt precipitation as it reaches the solubility limit. Recent studies conducted have proven that salt precipitation occurred due to CO_2 injection (Muller et al., 2009; Liu et al., 2013; Ott et al., 2015; Jeddizahed & Rostami, 2016).

The precipitated solids reduce the pore space available to the fluids and may block the pore throats, which subsequently hinder any further injection of carbon dioxide

(Muller et al., 2009). This condition will lead to permeability impairment associated with the multiphase flow and chemical reaction between CO_2, brine, and rock.
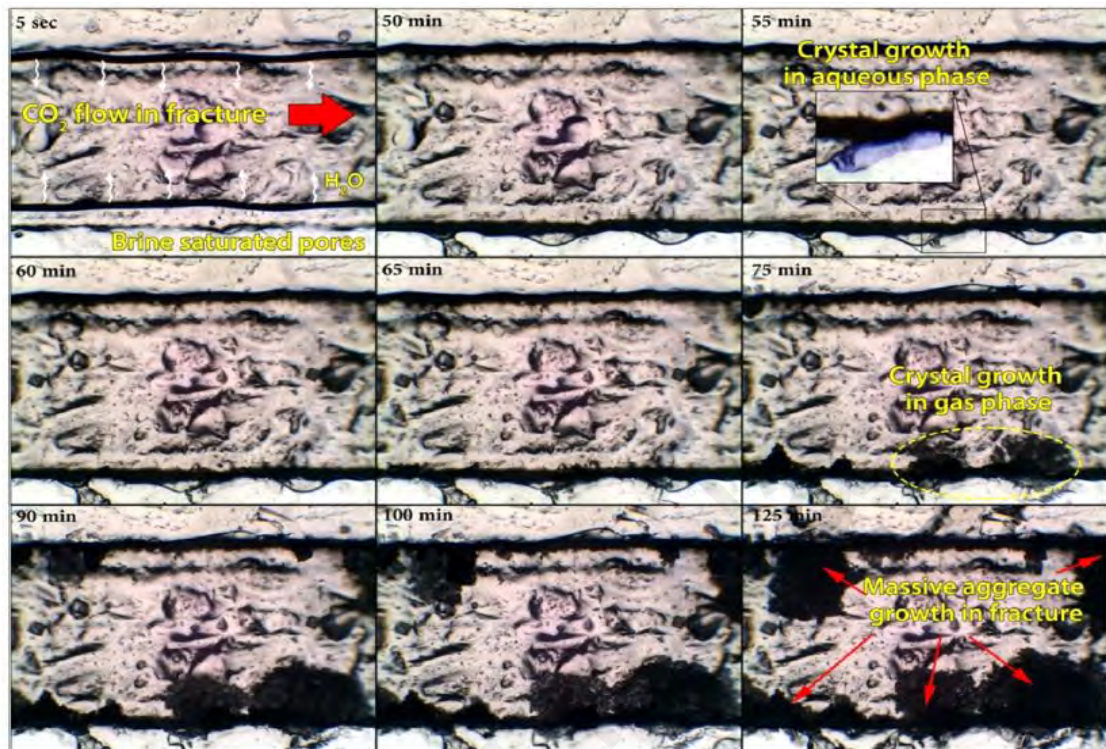
Figure 1.6: Pore-scale visualization of salt precipitation in the preferential pathway (fracture) of the heterogonous micro-chip. A thick film of brine remains after the CO_2 invasion at 5 s after injection. After 50 min, this film evaporates, and the drying front shapes a meniscus at the interface between matrix and fracture. At t = 55 min, large salt crystals form at several places inside the aqueous phase at interface between CO_2–brine (Miri et al., 2015).

The probability of water trapped in the pore throat in low-permeability water-wet formation is high and will cause permeability reduction (Nasr-El-Din et al., 2002). The capillary forces exerted between CO_2 and brine increases the severity of formation damage. Nevertheless, more damage is observed in heterogeneous rocks compared with a homogenous rock because its higher permeability value initiates more substantial precipitation reaction. CO_2 dissolves in the formation of brine, forming carbonic acid that dissolves carbonate mineral (Mohamed & Nasr-El-Din, 2013):

$$H_2O + CO_2 \leftrightarrow H_2CO_3 \tag{1.1}$$

$$CaCO_3 + H_2CO_3 \leftrightarrow Ca^{2+} + 2HCO_3 \qquad (1.2)$$

$$CaMg(CO_3)_2 + H_2CO_3 \leftrightarrow Ca^{2+} + Mg^{2+} + 2HCO_3 \qquad (1.3)$$
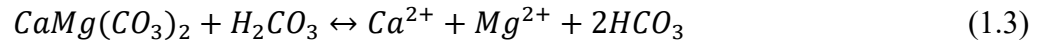
1.1.6 Scaling

Another issue attributed to CO_2 injection is the potential for scaling caused by incompatibility between CO_2 and the formation of water chemistry. If this problem is not addressed at an early stage, it could severely impact injection operations at the field scale level. $CaCO_3$ is the most likely scale for carbonate reservoir with the existence of other potential scales such as $BaSO_4$, $SrSO_4$, $FeCO_3$, and FeS. This work also investigated formation damage due to scaling and dissolution. Krumhansl et al. (2002) and Egermann et al., (2005) stated that formation brine might lead to calcium sulfate precipitation governed by Equation 1.4.

$$Ca^{2+} + SO_4^{2-} + xH_2O \leftrightarrow CaSO_4 \times xH_2O \qquad (1.4)$$
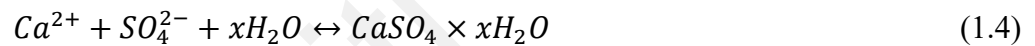
Where x is represents 0 for anhydrite, 0.5 for hemihydrate, and 2 for gypsum. The high fluid flow rate in the porous media was known as the main reason for fine migration in individual reservoirs (Miranda & Underdown, 1993). According to Wojtanowicz et al. (1987) and Nguyen et al. (2012), the critical flow rate/velocity may suspend fines or force them to move and deposit or bridge in the pore space and/or throat, which subsequently result in pore plugging.

Meanwhile, Miranda & Underdown (1993) proposed a unique method for determining critical rate by injecting fluid at a very low injection rate called baseline permeability and then the rate is increased in a step-wise manner. After that, the rate is returned to the initial rate (baseline permeability) after each incremental stage. Experimentally derived flow rate and permeability data are converted to the bottom hole and wellhead production rates using completion data and well geometry (Miranda &

Underdown, 1993). In-depth knowledge of flow during CO_2 injection is paramount to evaluate the feasibility of CO_2 sequestration in depleted carbonate field in Malaysia. To simulate the condition, coreflood testing using a multi-rate water-alternating-CO_2 (WAG) injection will be introduced to determine the critical rate for the investigated zone.

1.1.7 Storage Development Plan (SDP)

The first step in implementing a detail Storage Development Plan (SDP) for CO_2 sequestration in full-field scale is to conduct an SDP screening study that examines the field history data in terms of production, injection, pressure profile, and drives mechanism. Primary reservoir engineering data such as fluid and rock properties must be taken into account prior to CO_2 injection during the pilot phase.

Integration between full-scale projects and research is needed to gain knowledge and experience required for injectivity study. Typically, laboratory coreflooding experiments are designed and conducted to instigate further the efficiency of the CO_2 injection of the selected field. The assumption used for the laboratory coreflooding tests is that the reaction observed in laboratory analysis will be dominant in the long-term process.

The experimental study is essential to understand what would be happen at a microscopic level, hence, could significantly reduce the cost of injectivity study. If successful results are obtained from these coreflooding experiments, the study plan may proceed further in the field scale application but to be conducted in stages to minimize uncertainties such as pilot project and finally full-scale level if the project is found to be economically robust (Khanifar et al., 2015).

1.2   Research Objective

The general aim of this research is to have a better understanding on the feasibility study of CO_2 injection into a carbonate field from Sarawak, Malaysia. The water level in the reservoir has risen close to the cap-rock which implies potential problems relating to CO_2 storage, performance, and management of the gas reservoir such as:

   i.   Chemical interaction of the injected CO_2 and carbonic acid

   ii.   Degradation of the integrity of the near-wellbore condition by the injection operations

   iii. Formation damage that leads to a generation of new faults or CO_2 leakage

There have been numerous computer-based simulation studies conducted on the CO_2 sequestration subject incorporating carbonate and clastic formation. The published material on experimental studies is also available in the literature, but there are still various aspects of CO_2 injection, which require further analyses. The ultimate goal of this research is to evaluate the effect of CO_2 injection toward fluid experimentally and rock interaction by the potential chemical or physical process take place during CO_2 injectivity with the following specific objectives:

   i.   Investigating the critical rate of CO_2 injection into carbonate depleted field from Sarawak, Malaysia

   ii.   Investigating the geochemical effect of CO_2 injection toward carbonate formation

   iii. Investigating the porosity and permeability changes due to CO_2-brine-rock multiphase flow characteristic

CHAPTER 2: LITERATURE REVIEW

2.1 Introduction

In this research, a multi-rate CO_2 brine injection experiment was conducted to evaluate and understand the effect of CO_2 injection during carbon dioxide sequestration. In this study, the concept of relative permeability and capillary pressure should be exploited for a better description of the flowing fluids behavior and rock-fluid interaction. In the first part of this chapter, Darcy's Law will be introduced, while the second part of the chapter will be focusing on the carbonate rock from Central Luconia Province.

2.2 Darcy's Law

In the process of understanding this research, the multiphase flow through porous media using Darcy's equation is benchmarked for a single-phase flow of CO_2 and brine alternately. Darcy (1856) invented an empirical formulation for a linear flow, which has been a hallmark in modeling momentum transport through porous media. This equation is widely known as Darcy's law, whose convincing theoretical justification was proposed over 162 years ago that the fluid flow through porous media is a linear flow of a single-phase fluid under a constant pressure gradient. Nevertheless, several assumptions need to be understood to employ the equation in the form presented in the equation below. The assumptions are:

 i. The fluids flow exhibits fixed flow paths or laminar flow

 ii. Homogenous rock formation

 iii. Single phase fluid occupying 100% of the pore space

 iv. There are no chemical reactions between the fluid and the rock

$$q = -\frac{kA\Delta P}{\mu[L]}$$

(2.1)

Where q = fluid rate (cm^3/s), A = cross-sectional area (cm^2), μ = dynamic viscosity of flowing fluid (cp), and ΔP = pressure drop across porous medium (atm).

2.3 Carbonate

Carbonate sediments are commonly generated by direct precipitation out of seawater or by biological extraction of calcium carbonate from seawater to form skeletal material. This process depending on several factors, such as water temperature, alkalinity level, and dissolved ion concentrations.

There are two significant types of carbonate, namely limestone, and dolostone. Limestone is made of calcite/aragonite, while dolostone composed of the mineral dolomite. Minor components of carbonate rocks are made of siderite, gypsum, anhydrite, pyrite, phosphate, and glauconite. Carbonate is classified to make it easier for knowledge transfer, and frequently all classifications overlap and are unable to fit ones' particular needs. Carbonate commonly classified into two categories, which are Folk (1959, 1962) and Dunham (1962). These classifications are based on the matrix content.

2.3.1 Folk Classification

This classification usually applied if the rock contains over 10% allochems (transported carbonate grains). The rocks may be further subdivided into two categories, which are sparry allelochemical limestones and microcrystalline allelochemical limestone. Details studies on a further subdivision of Folk (1962) are shown in Scholle & Ulmer-Scholle, 2003.

2.3.2 Dunham Classification

This classification is identical to that of clastic rocks, except it displays the effect of energy towards sediment accumulation. The significant difference between rock types is based on the relative abundance of allochems (framework grains) and matrix. In Dunham classification, cement is considered an open pore space.

2.3.3 Depositional Environment

The depositional environment for carbonate can be categorized into three types, which are ramp continental margins, rimmed margins, and isolated platforms (Tariq Janj et al., 2017). Ramp continental margins are continental platforms gently sloping toward the ocean because of the high energy environment. The amplitude of the waves is higher as the sea depth getting lower. Meanwhile, the rimmed margins are formed by a steep & abrupt continental break. The structure is limited toward the ocean with a landward barrier having a low energy environment and oceanward having a high energy environment. Lastly, the isolated platform (Bahama type), which is characterized by the absence of siliciclastic input, is a shallow platform between 10 to 100 km wide continental shelves. The water depth usually ranges from 100 to 1000 m.
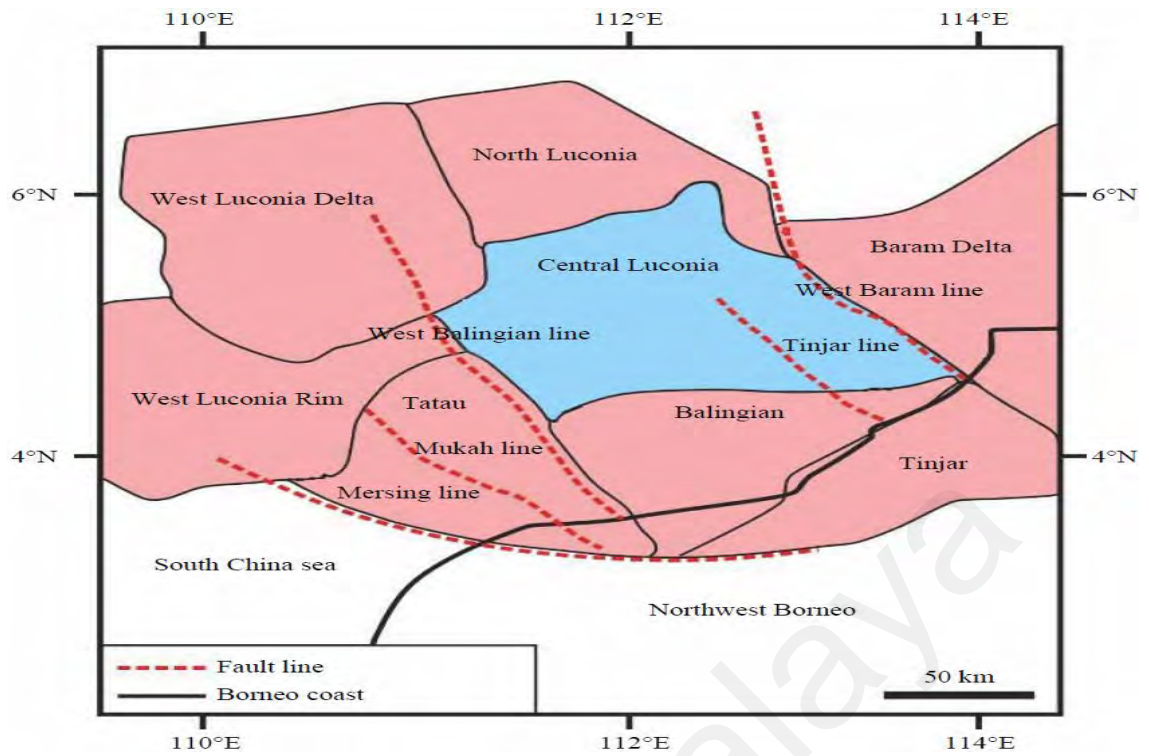
Figure 2.1: Central Luconia's structural map (Tariq Janj et al., 2017).

2.4   Geological Setting

The Central Luconia Province is located offshore Sarawak with an area of 200 km by 100 km of the outer half of the wide Sarawak shelf. The water depth is approximately 66 to 262 feet. It consists of several post-orogenic basins filled by predominantly siliciclastic sediments. Nevertheless, the Central Luconia Province is identified by the widespread development of Miocene carbonates. The west, south, and east boundaries are marked by Tatau Horst & Graben, Balingian, and Baram Delta, respectively, while the northern is enclosed by the present shelf edge. Structurally, Central Luconia is situated in the middle of subsidence and faulting in the north and Lower to Mid Tertiary compressional tectonics. The carbonate province underwent a low degree of structural deformation with moderate faulting during Oligocene to Lower Miocene. Movement during Lower to Middle Miocene for the second time induced basins and resulting morphology controlled the distribution of the subsequent prolific reefal carbonate growth.
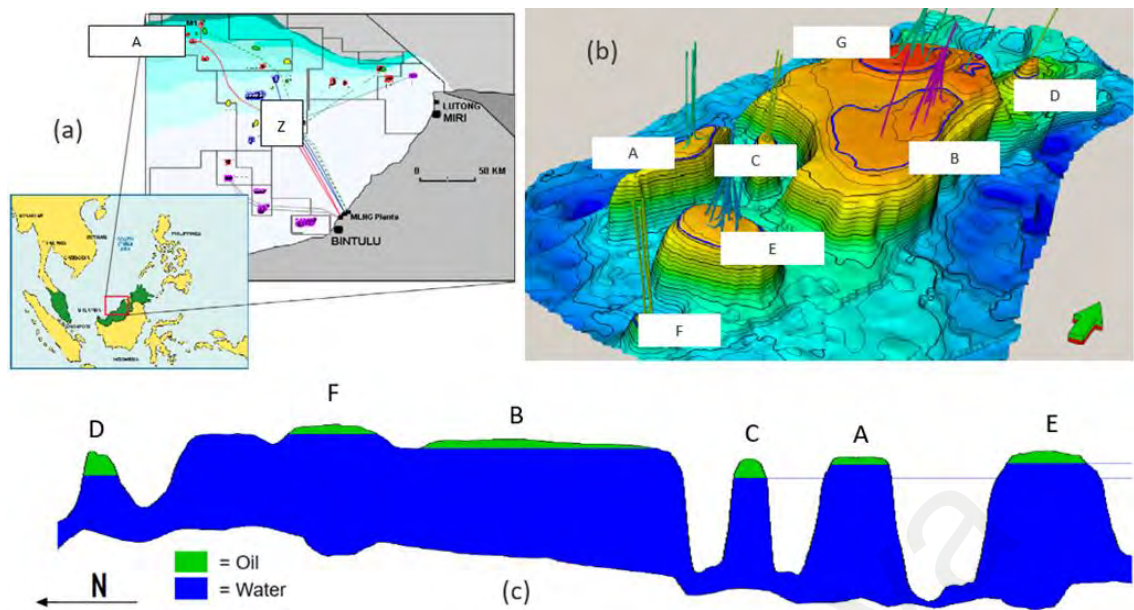
Figure 2.2: (a) Location map of A field in Sarawak; (b) Carbonates build-up structure; (c) Schematic cross-section of the mega platform and regional aquifer (Kok et al., 2003; Jalil et al., 2011; Masoudi et al., 2011; Masoudi et al., 2013).

The A field is located offshore Sarawak Basin, Malaysia, in the north of the Central Luconia province. Located about 253 km northwest from Bintulu Port, the field is about 6 km long and 2 km wide with a water depth of 117 m. The A structure is considered as a flat-topped, platform-type carbonate that builds up elongated in the north-south direction. This carbonate builds up field share common aquifer support with B, C, D, E, and an F field, which has a strong aquifer drive mechanism. Figure 2.2 depicted that the water level has risen up to the caprock level. Discovered by A-1 well in 1980, the field was then appraised by A-2 well in 1992, followed by A-101 and A-102 horizontal production well in 2002.

Stratigraphically, the reservoir intervals in the A field are in Cycle V in age with two depositional sequences, namely Alpha Build Up phase and Beta Build Up phase. Alpha Build Up phase carbonate sedimentation happened from low energy, deeper marine setting to the relatively higher energy of reefoid settings. Meanwhile, Beta Build Up

phase environment of deposition are predominantly protected to reefoid settings with some minor interval of shallow to deeper marine settings.
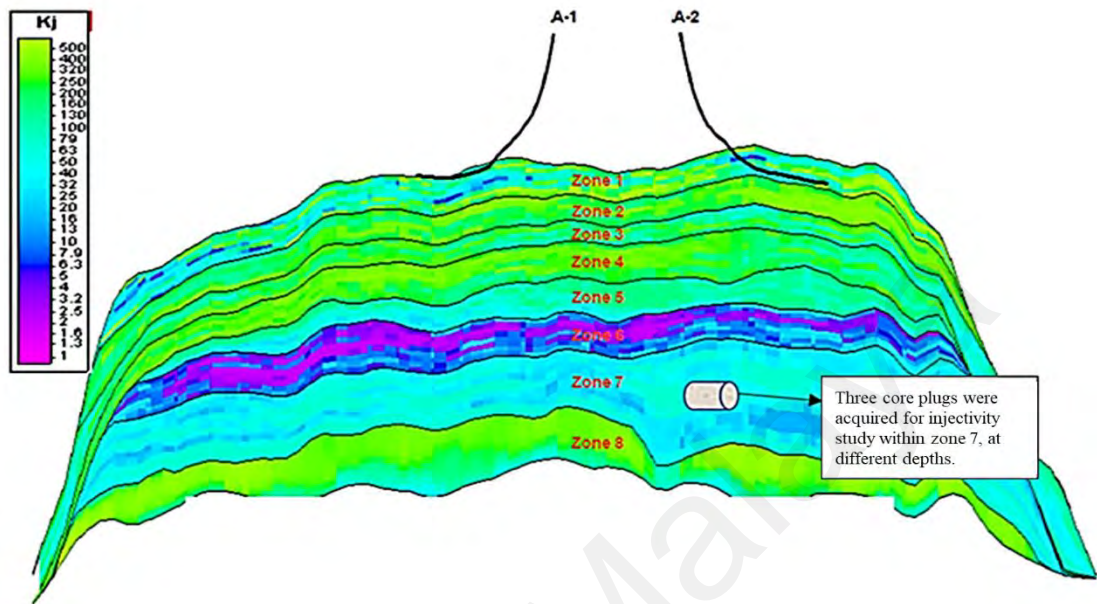
Figure 2.3: Location of A core plugs for injectivity study (Jalil et al., 2012).

The average porosity and permeability for Alpha Build Up phase is 30% and 273 mD, respectively. Meanwhile, the Beta Build Up phase shows average porosity and permeability of 32% and 242 mD, respectively. Zone 1 and 2 are within the Alpha Build Up phase, while zone 3, 4, 5, 6, 7 and 8 occur in the Beta Build Up phase. The location of the core was obtained from zone 7, refer Figure 2.3.

2.4.1   Sample Selection and Preparation

The first step in selecting representative core plug candidates was to conduct a physical check on the core samples. Core viewing activities such as core description and plug point screening were performed on the A-2 cores, which has a total length of 217 ft. The purpose of these activities is to familiarize with a geological setting, identify possible significant surface, and to understand the principal stratigraphic unit of this field. Based on the A-2 cores, there are several reservoir rock types classified according to the depositional and diagenetic process. The interpreted rock types in A-2 cores can

be categorized as 1) Mouldic Limestone 2) Chalky Mouldic Limestone 3) Chalky Limestone 4) Mouldic Dolomite 5) Mouldic Dolomitic Limestone 6) Chalky Dolomitic Limestone.

Thenceforth, the conventional core image was captured using a CT scanner to determine the best location for core plug selection. Nine core plugs samples were chosen from A-2 well for the low, mid, and high case. These cases represent different permeability conditions observed during a core viewing session. Plug points were then selected based on the core condition where the core was coherent without visible fracture, location of planned CO_2 injection, and petrophysical properties incorporating porosity and permeability range. Based on the cored section of A-2 well, the porosity range was between 24% to 40%, while the permeability range was between 150 mD to 1100 mD. One of the significant tasks performed during an inspection of the core was to ensure the labeling of the core sheets with the correct driller's depths for the cored interval as well as relevant well data. It is essential to have representative wireline log prints over the cored section. Figure 2.4 represents the wireline log on the cored section of the A-2 well.
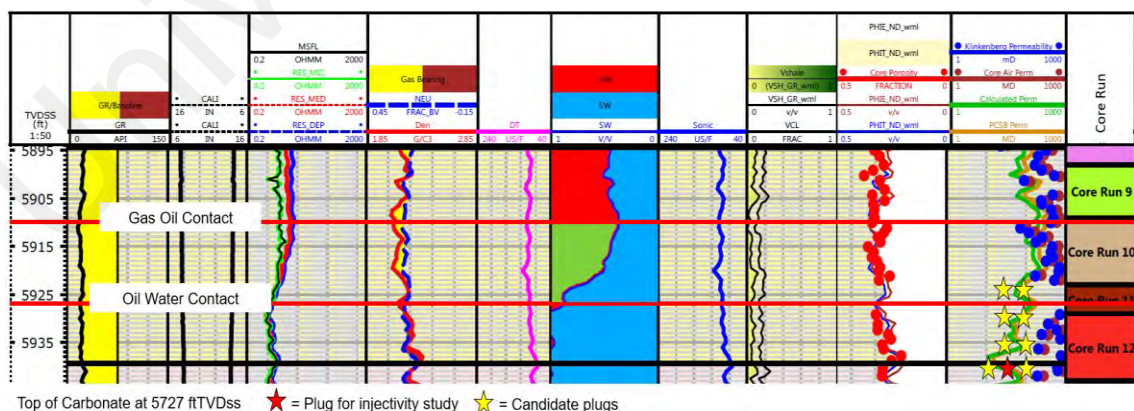
Figure 2.4: Log analysis at sample points (Copyright permission from PETRONAS).

Since core gamma was unavailable to match the driller depth with log depth, porosity versus permeability data was applied, resulting in 5 ft differences between the depth references. One of the limitations encountered during this process was that the available wireline log and core data were captured before the water had risen to the caprock. Ideally, it is better to obtain log data and core data after the field had been identified as a depleted field.
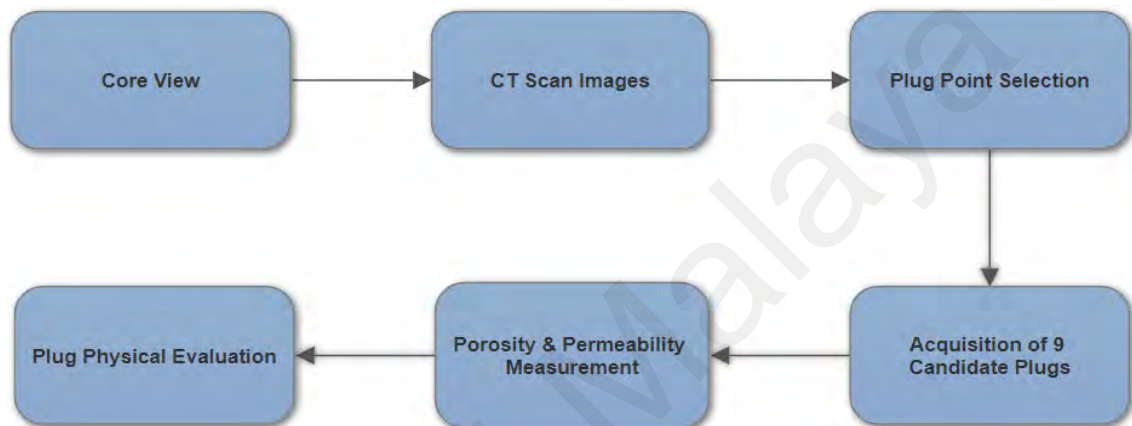
Figure 2.5: Process workflow for core selection.

Nevertheless, due to the unavailability of well-drilled after the field was depleted, the existing core plug acquires during appraisal activities had been utilized for this study. After obtaining samples for the injectivity study, the core plugs were sent for the core cleaning and drying process before porosity and permeability measurement using a porosimeter. Figure 2.5 shows the process workflow for core selection.

The core view was performed at PETRONAS Geo-Sample Centre, Kuala Lumpur. CT scan images of the core plugs were analyzed, and plug points were selected with petrophysicist discipline expert. Nine candidate plugs were selected for porosity and permeability measurement, but only three core plugs were used for the main experiment based on the plug physical evaluation.

2.5   Research workflow

The workflow for this research is summarized in the following chart. Knowing the geological and reservoir summary of the core plug origin is very critical at the early stage of the study. After gathering data, information, and methodology for this project, sample selection and preparation were conducted for the primary purpose of this research, which has been written in blue boxes. Routine core analysis is undertaken to determine the density, porosity, and permeability of core plugs samples prior to the main experiment.
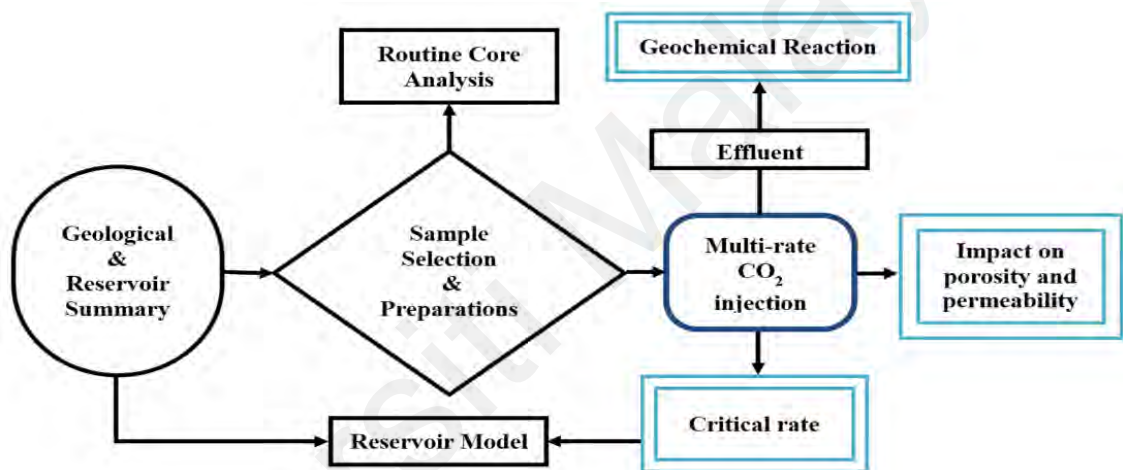
Figure 2.6: Research workflow.

The main experiment for this project is the coreflooding experiment or also known as multi-rate CO_2 injection. Based on this experiment, the main objectives of this research can be met which are geochemical reaction, critical rate, and changes in porosity and permeability value due to CO_2 injection. Critical rate value is validated with the existing reservoir model.

CHAPTER 3: METHODOLOGY

3.1   Introduction

A significant part of the experimental work related to this research was carried out using state of the art, high-pressure high-temperature core-flooding apparatus located within the PETRONAS Research Sdn. Bhd. To achieve the objectives of this study, thorough discussion and various types of flooding experiments were designed and implemented. This section contains three main parts which:

  i.   The first part will be regarding the detailed explanation about the experimental apparatus and its functions

 ii.   The second part is regarding the types of materials such as fluids and core samples used during the experiments

iii.   The third part will be about the experimental procedures of all the laboratory works

3.2   Experimental Apparatus

The maximum allowable pressure and temperatures for the core-flooding apparatus are 15,000 psi and 200°C, respectively. This equipment capable of performing a wide range of core-flooding related research within one stand-alone integrated system. The system is applicable for all main multiphase flow experimental studies such as EOR related research, formation damage analysis, and CO_2 injectivity study. The most significant wetted metal parts of the apparatus are made of highly resistant material such as Hastelloy and stainless steel to cater to the corrosive effect of CO_2 and H_2S. This feature enables the equipment to be rust free and corrosion resistant even under high-temperature environments with high chloride concentration.
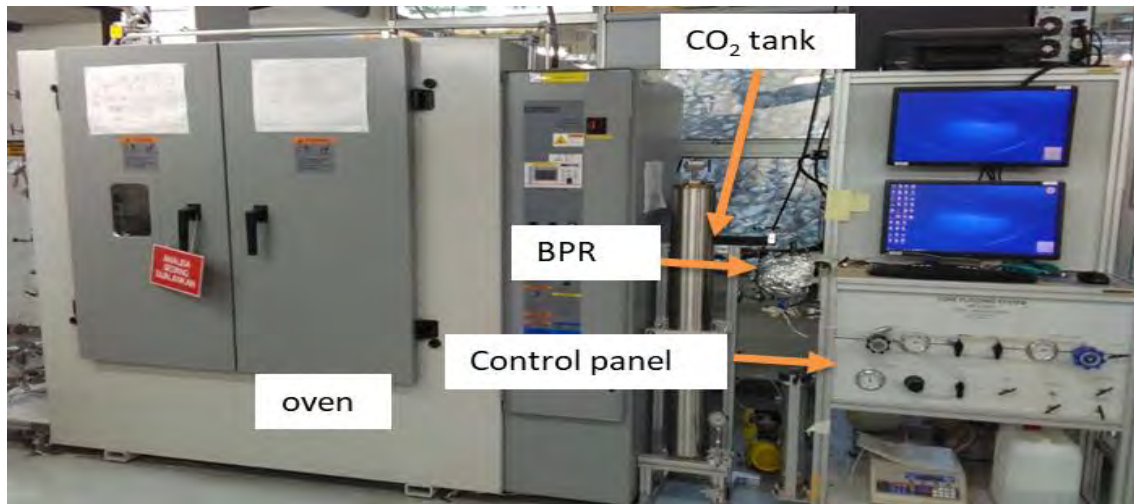
Figure 3.1: Complete system of coreflood.

In Figure 3.1, the oven is located on the left side while the computer used for data logging is placed on the right side. The blow out preventer (BPR) is wrapped with aluminum foil to maintain the reservoir temperature inside the system. CO_2 tank is situated between the oven and computer to utilize the room space. The high-pressure pump is used to minimize the time required to transfer CO_2 from the main tank to the tank in Figure 3.1. To comply with Health Safety Environment (HSE) department requirement, a tag showing whether the equipment is in operation or not is hanging outside at the oven's door.
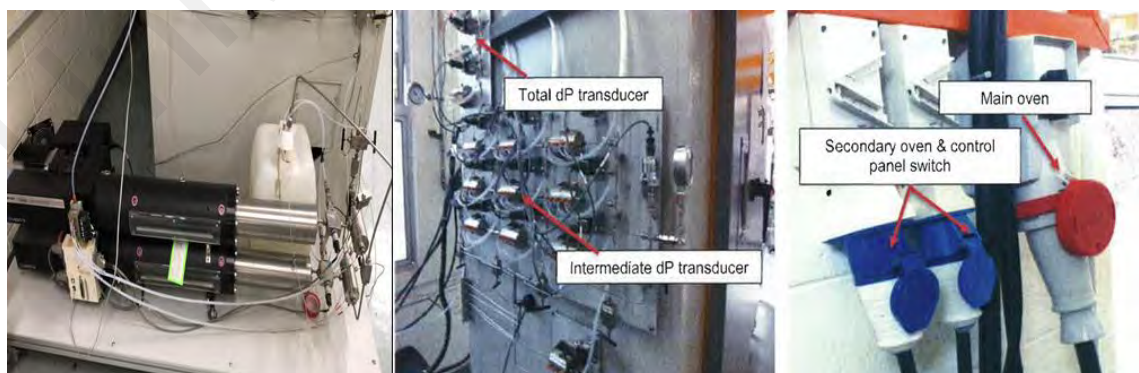
Figure 3.2: Quizzix pump (left), hydraulic fluid, ΔP transducer and power supplies.

Figure 3.2 represents ΔP transducers, which act as valves to monitor the differential pressure across the system while power supplies control electricity to oven and computer.
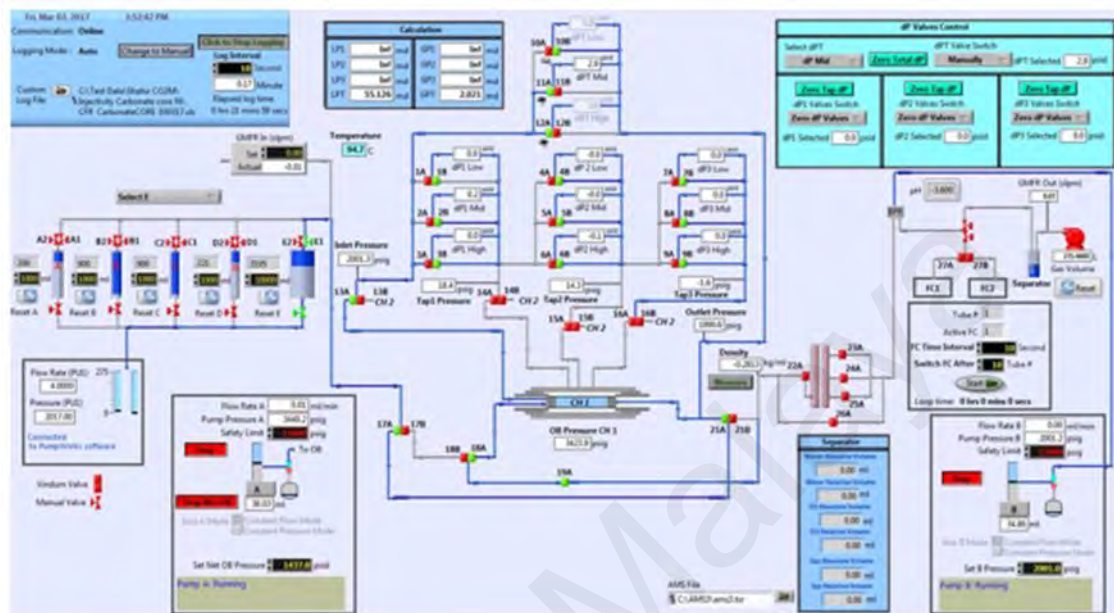
Figure 3.3: The schematic diagram of the experimental apparatus.

All the wetted parts carrying fluids during testing are located inside a huge constant temperature convection oven. The room is also equipped with a ventilation system to circulate the hot air out of the room. The CO_2 accumulator is placed outside the oven. In short, the system comprises four main sub-systems, the injection system, the core holder, the separation and collection system, and the data logging and monitoring system.

3.2.1 The injection system

As shown in Figure 3.3, the injection system consists of two main components, which are the injection pump and the fluid accumulators. The injection pump is capable of working under various injection conditions, constant flow rate, constant pressure, constant pressure with adjustable pressure ramp, and reaching a target

injection volume. The pump is connected to the fluid accumulators and the hydraulic fluid storage tank through connecting valves that will open or close through air pressure. Each accumulator contains a floating piston that is used to separate the hydraulic fluid with the injection fluid. The fluid accumulator A through D has a capacity of 1,000 ml each and accumulator E has 10,000 ml capacity. Usually, in PETRONAS Research Sdn Bhd (PRSB), accumulators A through D will be filled with brine however, accumulator E will be strictly filled with a gas such as CO_2. Thus, the capacity of all the accumulators will be sufficient to conduct a steady-state flow experiment using an average permeability core sample without any interruption.

3.2.2   The core-holder

The core holder used during this experiment has identical axial and radial confining pressure through annular space along the outer diameter of the core sample. Two confining pressure ports are provided so that the annular space between the core-sample and the inner diameter of the core-holder body can be filled with overburden fluid using one of the ports while the air is easily expelled from the other (Saeedi, 2012).
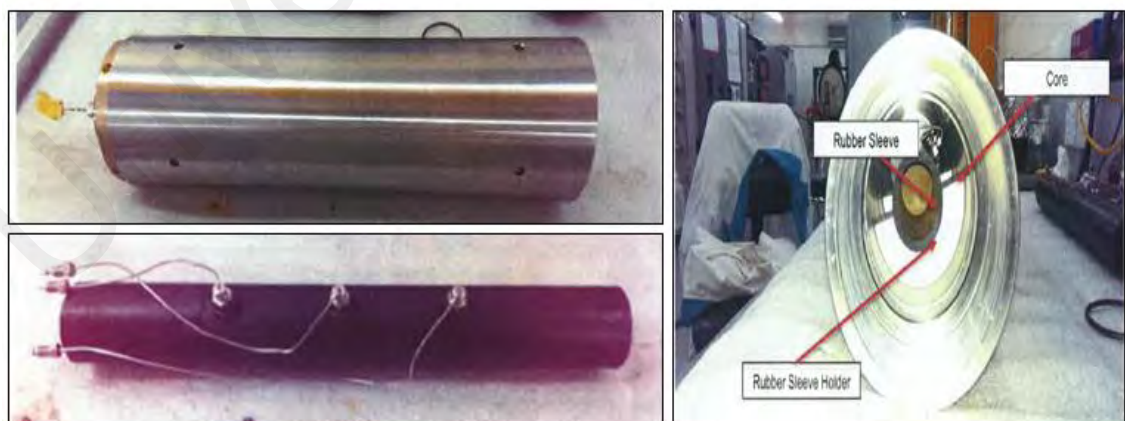
Figure 3.4: The core holder on the upper left, rubber sleeve to the inlet lit of core holder on the below left and a cross-sectional view of the core holder on the right.

In order to allow the core plug, remain in constant contact with the core holder as pressure is applied, the outlet distribution is connected to a rubber sleeve located in the

center of the end cap. This tube can slide back and forth as required. The volumes of all ports and flow lines have been kept to a minimum to reduce the system dead volumes and improve the volume measurement accuracies.

3.2.3 The separation and collection system

The separation and collection system comprised of a pump, sensors, and separator. The effluent is passing through BPR into separator due to gravity inside the specially designed separator. After the BPR, the system is at ambient condition. Material balance calculation is taken into account to back-convert the produced volumes to reservoir conditions. Furthermore, for the experiments carried out during this research, the produced CO_2 is sucked by a wet test meter while the effluent is collected in an air-tight jar.
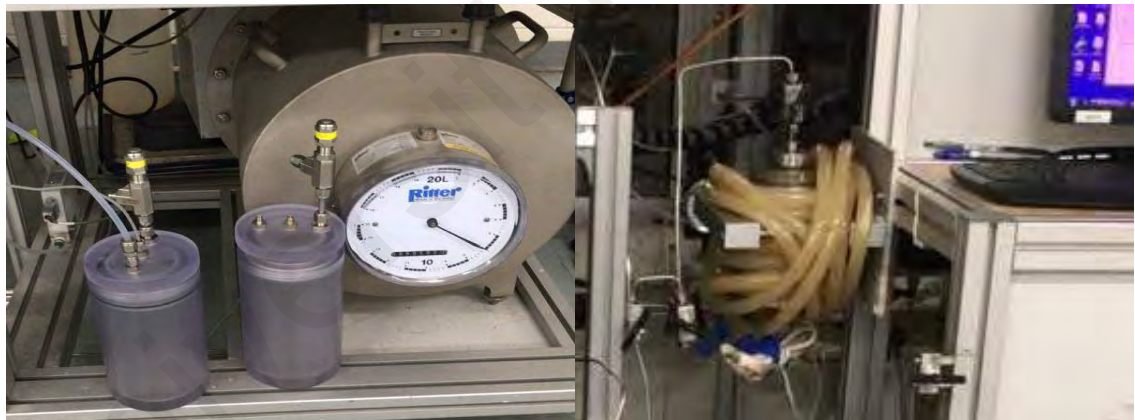
Figure 3.5: Wet test meter, effluent collector and BPR.

3.2.4 The data logging and monitoring system

All components of the apparatus are connected to a computer with appropriate data logging and monitoring software installed. The whole system, including the sensors, the Piping and Instrumentation Diagram (PID) controllers, the injection and collections pumps, and the pneumatic valves, are monitored and controlled using this computer (Saeedi, 2012). The data logging was conducted with time-steps as short as one second.

3.3   The Material

3.3.1   Fluids

In total, three different types of fluids were used during various stages of the experimental work. These fluids included dead brine (brine with no dissolved gas content), supercritical CO_2, and distilled water. The CO_2 gas applied was of a bottled high-purity grade (99.99%) carbon dioxide. The synthetic brine was prepared in the preparation room using distilled water and sodium chloride (NaCl).

3.3.2   Core Samples

The core samples used during this experimental work were all carbonate. They were chosen from several varieties to cover a range of carbonate types present in such geological structures. The core samples could be divided into three different groups based on their porosity and permeability range.

3.4   Experimental Procedure

All the core plugs used for this experiment followed a standard operating procedure that has been outlined in the literature. Apart from the coreflooding experiments which constituted the core of this research, there was a variety of other experimental and preparation work carried out as well, which included (Saeedi, 2012):

i.   Sample selection at warehouse

ii.   Core cleaning and drying of any possible hydrocarbon, salt, and drilling mud residues

iii. Porosity, permeability, grain density, and water permeability

iv.   Aging the samples in dead brine to restore their original wettability

3.4.1   Core Plug Preparation and Preliminary Measurements

Core allows researchers to examine rock matrix properties and formation characterization. This process is vital to evaluate porosity, permeability, fluid saturation, grain density, lithology, and texture. These analyses are commonly known as routine core analysis. The core plugs were cut using a pedestal press drill with 1.5" inner diameter coring bit using freshwater. This size was selected to match the core holder size that caters to 1.5" diameter core plug. Coring using fresh water may affect formation damage due to clay swelling, severe contamination, and wettability alteration while the operation takes place. However, the core plugs were still taken using fresh water since the core plugs tend to break while coring activity conducted. The core plugs will undergo a sample restoration process prior to coreflooding experiment. After the coring, the end faces of the core plugs were trimmed and smoothed to ensure proper contact between the core holder end plugs and the end faces of the core samples to eliminate any capillary discontinuity (Saeedi, 2012).

The core plugs were cleaned of any possible residual hydrocarbons and drilling mud using toluene at 140℃ while methanol at 90℃ to remove possible salt precipitation. Cold soxhlet was used for the purpose of core cleaning for this research. The reflux process was maintained until the color of the condensed solvent mixture remains constant. Depending on the permeability of the samples, the cleaning time varied from two to fourteen days. Special care was always taken not to overheat the samples to avoid core damage. After the samples were left for 24 hours to remove bad odor, a drop of silver nitrate was inserted into the effluent. The core samples are considered clean once clear solution formed. Thenceforth, the core samples were transferred to humidity oven for humidity drying at 60℃ for 24 hours prior to RCA measurement. Humidity drying was selected over hot drying to preserve the sample mineralogy if any fibrous

illite presence in the core samples as hot drying method could cause damage to fibrous illite.

The core cleaning is considered successful when the core is left strongly water-wet because almost all clean reservoir minerals are strongly water-wet (Gant & Anderson, 1988). There are several methods to clean core sample such as distillation/extraction (Dean-Stark and Soxhlet), flow through core cleaning, & centrifuge flushing (Gant & Anderson, 1988; RP40, 1960) Nevertheless, wettability is a function of rock mineralogy, oil composition, brine composition, pH, reservoir pressure, reservoir temperature and also thickness of connate water layer. Theoretically, a reservoir composed of calcite (carbonate) is more likely to be oil-wet (mix wettability) than those composed of silica (sandstones) for the oil reservoir. In this study, the focus is purely on carbonate rock for gas and aquifer core plugs. Therefore, the core cleaning is considered successful when the core is left strongly water-wet rather than mixed wettability.

Unsteady state measurement using Coreval 700 equipment was used for calculating the permeability, porosity, and grain density. This unsteady state measurement incorporated a pressure falloff technique where the downstream outlet port was vented to the atmosphere. The tests were conducted using Nitrogen as flowing fluid. Note that, although the initial net overburden pressure is set at 800 psig, it varies both spatially and temporally during the unsteady-state measurements (Rushing et al., 2004).

Figure 3.6: Cold Soxhlet and RCA.

3.4.2 The Coreflooding Experiments

3.4.2.1 The Coreflooding Procedure

This experiment practiced the approach of WAG injection of CO_2 concept rather than simultaneous water and CO_2 injection schemes. A higher percentage of CO_2 were stored by residual trapping under WAG injection based on a study conducted by (Juanes et al., 2011). The first step to prepare coreflooding experiment was to measure the dry weight, length, and diameter of the carbonate core plug. The sample was immersed in synthetic brine at ambient condition and vacuumed until no bubble was released from synthetic brine.

Thenceforth, the selected core plug was pressurized for 36 hours at 1 000 psi in an accumulator to remove the gas trapped in the pore space. After the measurement of wet weight of the saturated core plug, we calculated the pore volume based on Equation 3.2, where π equivalent to 3.142, r, and L is the core plug radius and length in cm, respectively. In this calculation, water density is assumed to be 1 g/cc.

$$\text{Pore Volume,} \quad PV \; (cc) = \frac{Saturated \; weight \; (g) - Dry \; weight \; (g)}{Brine \; density \; (g/cc)} \qquad (3.1)$$

$$\text{Bulk Volume,} \; BV \; (cc) \; = \; \pi \times r2 \times L \qquad (3.2)$$

$$\text{Porosity,} \; \theta \; (\%) \; = \; \frac{PV}{BV} \times 100 \qquad (3.3)$$

Brine permeability (Kbrine) must be established prior to the WAG injection of CO_2. The chosen brine rates for this purpose are at 0.5 ml/min, 1.0 ml/min, and 1.5 ml/min. After Kw was obtained, it was advisable to use ΔP corresponding to a flow rate of 1.0 ml/min as a baseline. CO_2 was flowed from top to bottom of core holder at an identified flow rate and constant volume until it reached stabilized ΔP. The core was then saturated back by injecting the brine from bottom to top of core holder at a constant flow rate of 1 ml/min to restore initial reservoir condition of the core. This process was repeated until the CO_2 flow rate unable to reach stabilized ΔP. The effluent and gas produced at each step were collected for material balance calculation and interpretation.

Saeedi (2012) suggested placing the core-holder containing the sample in a vertical position where CO_2 is injected from top to bottom while brine is injected from bottom to top to eliminate the effect of gravity segregation (underrun or override of the injected fluids).

Core holder and brine accumulator were located within an oven at in-situ reservoir condition. CO_2 accumulator was placed outside the oven at the ambient condition to prevent CO_2 expansion for safety purposes. Corrected flow rate injection was incorporated using the Charles Law equation to reduce the experimental error produced during laboratory analysis. Figure 3.7 and Figure 3.8 are schematics of the setup used for the coreflood test.
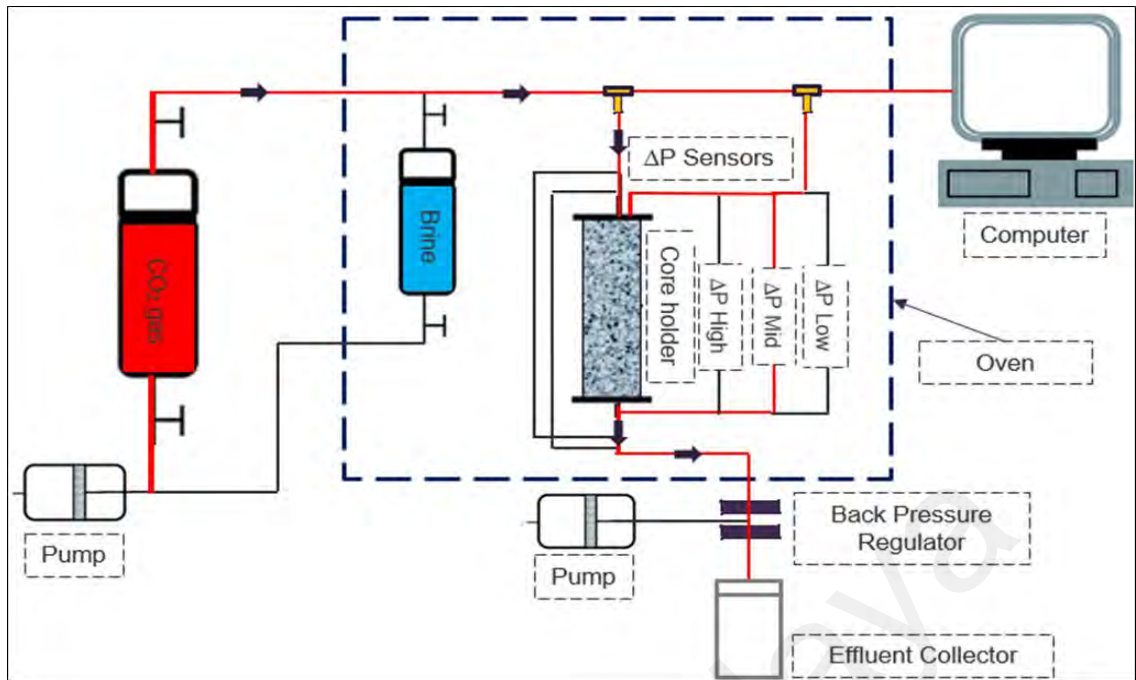
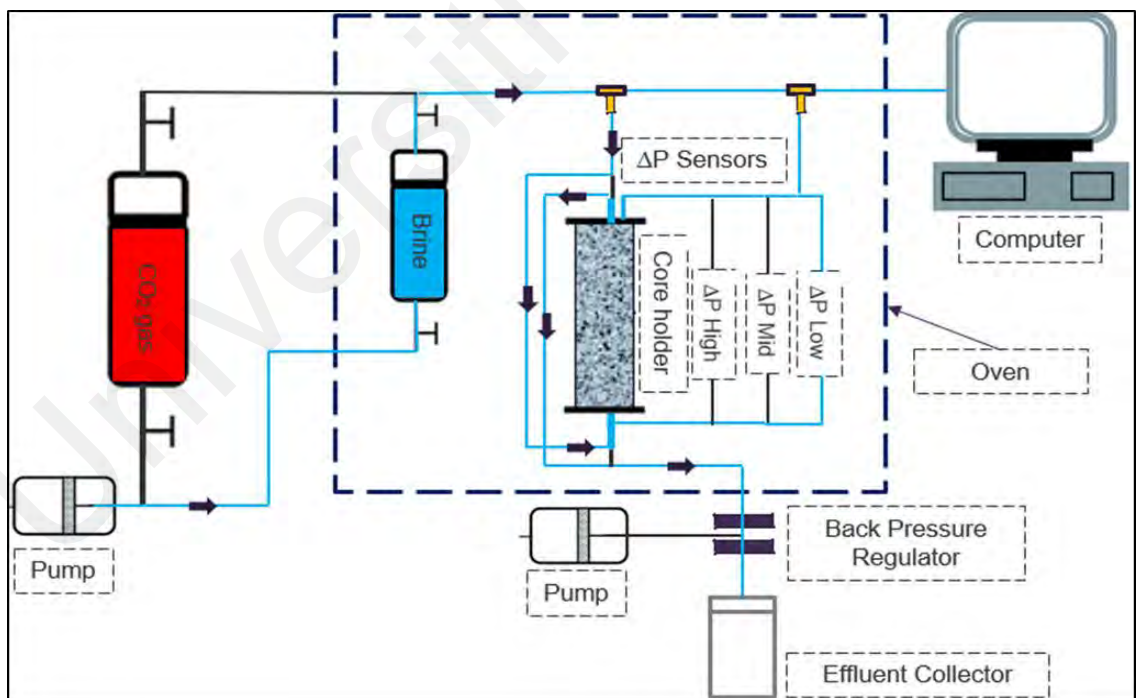**Figure 3.7: CO₂ injection flow (red) diagram inside coreflood system.**

Figure 3.8: Brine injection flow (blue) diagram inside coreflood system.

CHAPTER 4: RESULT

4.1   Introduction

As mentioned in the previous chapter, to achieve the research objectives, various types of laboratory work were conducted during the development of this study program. The experimental work carried out ranged from sample preparation, routine core analysis to core flooding test. This chapter presents in detail the results of the various laboratory tests performed.

The result presented in this section covered the work from fundamental physics of the core samples used, such as X-Ray Diffraction (XRD) analysis, Scanning Electron Microscope (SEM), RCA, brine and effluent result from the investigated samples. The results of the coreflooding experiments carried out are presented in this chapter, as well.

4.2   Lithology Analysis

A total of 30 feet of the aquifer core samples were taken consists predominantly of Mouldic Limestones with a minor interval of Chalky and Mouldic Limestone. The faunal assemblages indicate a range of deposition from protected/reefoid to deeper marine. The samples consist of highly porous, slightly recrystallized boundstones made of coral, algal, and calcareous skeletal particles cemented by sparry calcite.

Table 4.1 and Table 4.2 showed the weight percentage of rock and clay composition for nine candidate core plug samples that are representative of the aquifer zone based on XRD analysis. There are only three of them are selected for injectivity study, namely sample 1, sample 2, and sample 3. These tables have shown that total clay is less than 10%, mostly illite, mixed-layer I/S, kaolinite, chlorites, and smectite. Calcite dominated the total of the rock composition at approximately 80% of total weight percentage.

Table 4.1: Rock composition.
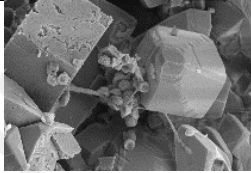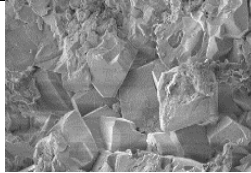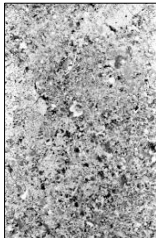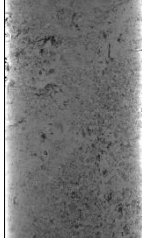
No	Quartz	Plagioclase	K Feldspar	Calcite	Dolomite	Siderite	Pyrite	Total Clay	TOTAL
1	0.3	2.1	2.1	80.1	7.3	0.9	1.4	5.8	100
2	0.4	2.3	3.1	84.9	1.3	0.8	1.8	5.4	100
3	0.5	2.2	2.2	81.7	3.4	0.9	1.6	7.5	100
4	0.4	2.5	2.8	80.0	3.0	1.0	2.1	8.1	100
5	0.5	2.5	2.8	80.5	4.3	1.0	1.7	6.7	100
6	0.4	2.6	2.3	81.7	3.8	0.9	1.6	6.6	100
7	0.7	2.7	2.9	77.2	5.2	1.0	2.1	8.2	100
8	0.4	2.4	3.2	81.5	3.5	1.0	1.7	6.2	100
9	0.4	2.5	2.6	78.2	5.9	0.9	1.8	7.7	100

Table 4.2: Clay composition.
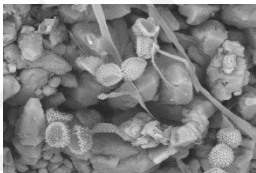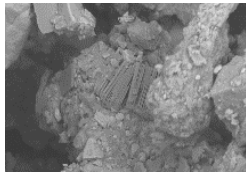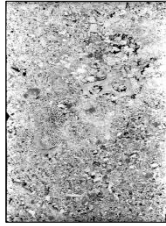
No	Kaolinite	Chlorite	Illite	Mixed Layer	Smectite
1	12.9	7.8	53.2	21.1	4.5
2	12.6	7.0	56.2	17.9	6.1
3	13.5	8.0	51.4	22.5	4.9
4	12.2	6.6	58.3	18.0	4.9
5	12.4	7.4	57.8	18.4	4.4
6	13.6	7.2	53.7	20.8	4.9
7	12.8	8.1	52.8	20.8	5.2
8	13.5	8.4	50.2	22.9	5.1
9	13.4	7.8	51.9	22.1	4.9

The pre-post summary for selected injectivity core plug samples is tabulated in Table 4.3, 4.4, and 4.5.
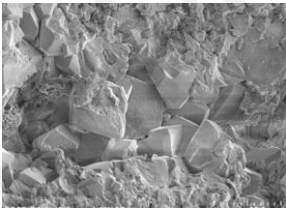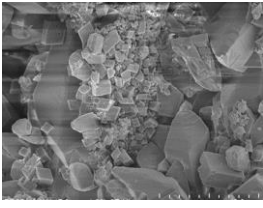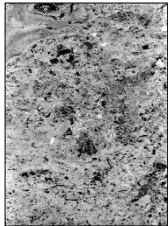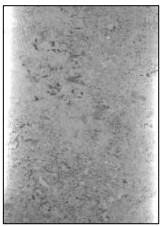
Table 4.3: Comparison pre-post CO₂ injection for sample 1.

Sample	1			
Carbonate Classification (Dunham 1962)	Boundstone			
Sample Condition	Pre-CO₂ Injection		Post-CO₂ Injection	
% Calc Skelatal Grains	10.5		3.2	
% Calcite spar (>10 m)	19.2		29	
% Microspar (>10 m)	45.4		43.9	
% Dolomite	0.8		1	
% Clay	0.1		0.1	
% Modal Porosity	26		25	
Carbonate Grain types	coral, foraminifera and red algae			
Authigenic Cements Types	minor dolomite, sparry calcite			
Clays	non observed			
SEM Image	20 μm		30 μm	
Dominant Pore Types	Intercrystalline, Dissolution			
Core Plug Photo	Length (in.)	Diameter (in.)	Length (in.)	Diameter (in.)
	2.9	1.5	2.9	1.5
Micro-CT Image (39 micron)				
Pre-Post comparison	No significant change in texture or morphology			

Table 4.4: Comparison pre-post CO₂ injection for sample 2.

Sample	2	
Carbonate Classification (Dunham 1962)	Boundstone	
Sample Condition	Pre-CO₂ Injection	Post-CO₂ Injection
% Calc Skelatal Grains	15.0	7
% Calcite spar (>10 m)	36	33
% Microspar (>10 m)	25	34
% Dolomite	0.85	1
% Clay	0	0
% Modal Porosity	23	21
Carbonate Grain types	coral, foraminifera and red algae	
Authigenic Cement Types	minor dolomite, sparry calcite	
Clays	non observed	
SEM Image	20 μm	30 μm
Dominant Pore Types	Intercrystalline, Dissolution	

Core Plug Photo	Length (in.)	Diameter (in.)	Length (in.)	Diameter (in.)
	2.9	1.5	2.9	1.5

Core Plug Photo		
Micro-CT Image (39 micron)		
Pre-Post comparison	No significant change in texture or morphology	

Table 4.5: Comparison pre-post CO₂ injection for sample 3.

Sample	3	
Carbonate Classification (Dunham 1962)	Boundstone	
Sample Condition	Pre-CO₂ Injection	Post-CO₂ Injection
% Calc Skelatal Grains	5.0	2.5
% Calcite spar (>10 m)	25	37.5
% Microspar (>10 m)	50.1	38.7
% Dolomite	0.4	0.66
% Clay	0	0
% Modal Porosity	21	22.4
Carbonate Grain types	coral, foraminifera and red algae	
Authigenic Cement Types	minor dolomite, sparry calcite	
Clays	non observed	
SEM Image	 30 µm	 40 µm
Dominant Pore Types	Intercrystalline, Dissolution	
Core Plug Photo	**Length (in.)** | **Diameter (in.)** 2.9 | 1.5 	**Length (in.)** | **Diameter (in.)** 2.9 | 1.5
Micro-CT Image (39 micron)		
Pre-Post comparison	No significant change in texture or morphology	

4.3   RCA

This section represents RCA for all candidates' plugs. The net confining stress is conducted at two different values which are at 800 psi and 1200 psi. The accuracy of these data is validated based on sensitivity analysis shown in Figure 4.1 until 4.3. Permeability versus porosity plot gives an insignificant different value between two net confining stresses. Therefore, these data are representative to be used as a guideline for injectivity study. Looking at Figure 4.1 until 4.3, these points fall on the acceptable range of the straight line (±10%); hence these data are considered correct.

Table 4.6: Routine Core Analysis Result.

No	Net Confining Stress				Net Confining Stress			
	800 psi				1200 psi			
	Grain Density (g/cc)	Kair (mD)	Klinken berg (mD)	Porosity (%)	Grain Density (g/cc)	Kair (mD)	Klinken berg (mD)	Porosity (%)
1	2.71	213	172	26	2.71	208	158	26
2	2.71	123	81	29	2.71	122	78	29
3	2.71	1824	1769	30	2.71	1744	1691	30
4	2.71	56	43	31	2.71	55	43	31
5	2.71	457	435	30	2.71	416	395	30
6	2.72	244	115	30	2.72	240	107	30
7	2.71	273	211	27	2.71	271	204	27
8	2.71	2046	1986	29	2.71	1958	1901	29
9	2.71	1084	1045	28	2.71	1046	1008	27

Data tabulated in table 4.6 are plotted in Figure 4.1 for permeability versus porosity to highlight the sensitivity analysis for these data. Since the overlapping orange and yellow circle are not far off and within an acceptable range, these data taken at two net confining stress is considered correct.
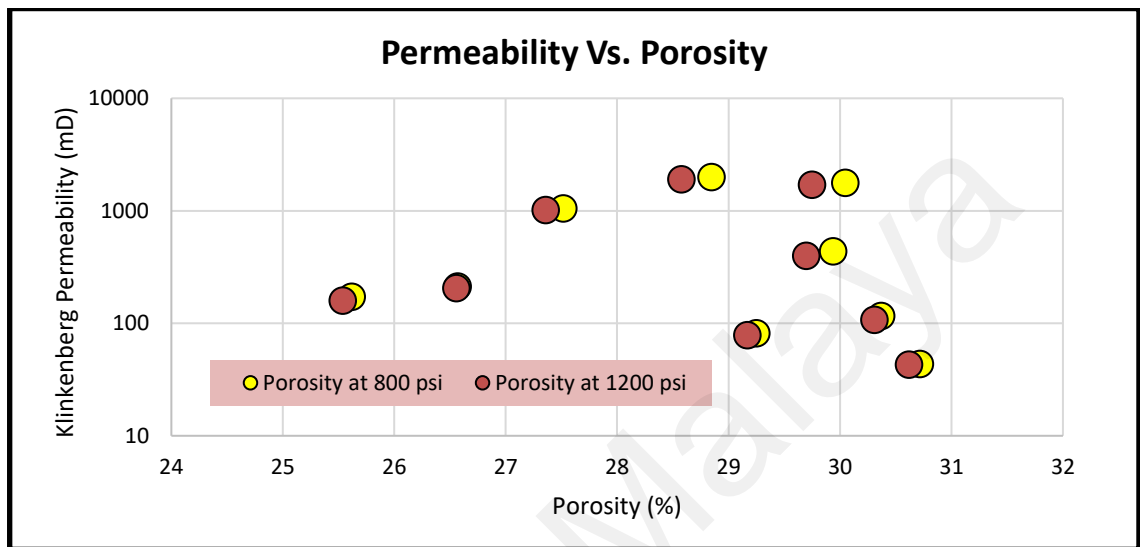
Figure 4.1: Permeability vs. porosity sensitivity analysis.

Data tabulated in Table 4.6 are plotted in Figure 4.2 for air permeability versus Klinkenberg permeability to highlight the sensitivity analysis for these data. Since the overlapping green and yellow circles are not far off from the red line and within an acceptable range, these data taken at two net confining stresses are considered correct. If the plotted orange and yellow points are not overlapping, it means the core is not suitable to be used for further analysis.
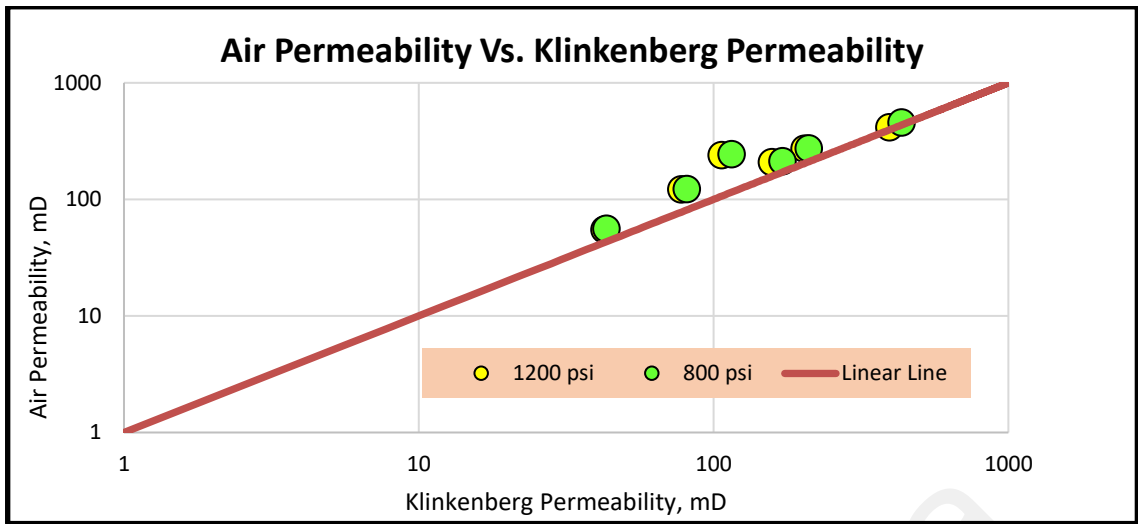
Figure 4.2: Permeability sensitivity plot.

Data tabulated in Table 4.6 are plotted in Figure 4.3 for porosity measurement at 800 psi versus porosity measurement at 1200 psi to highlight the sensitivity analysis for these data. Since these data are on the red line, the readings are considered correct.
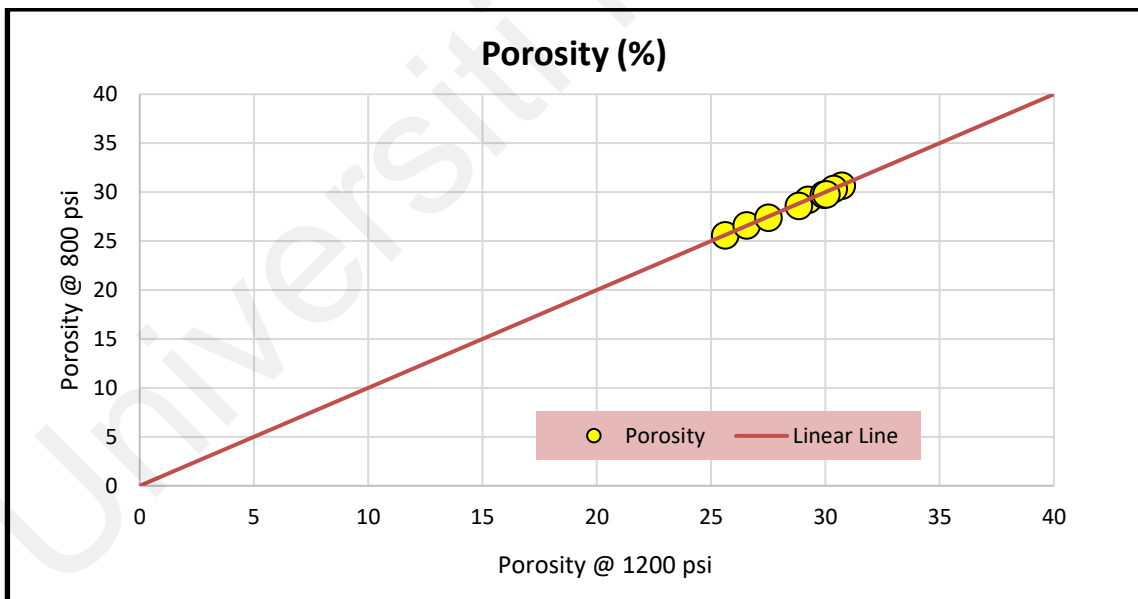
Figure 4.3: Porosity sensitivity plot.

Data tabulated in Table 4.6 are plotted in Figure 4.4 for grain density at 800 psi versus at 1200 psi to highlight the sensitivity analysis for these data. Since these data are on the red line, the readings are considered correct.
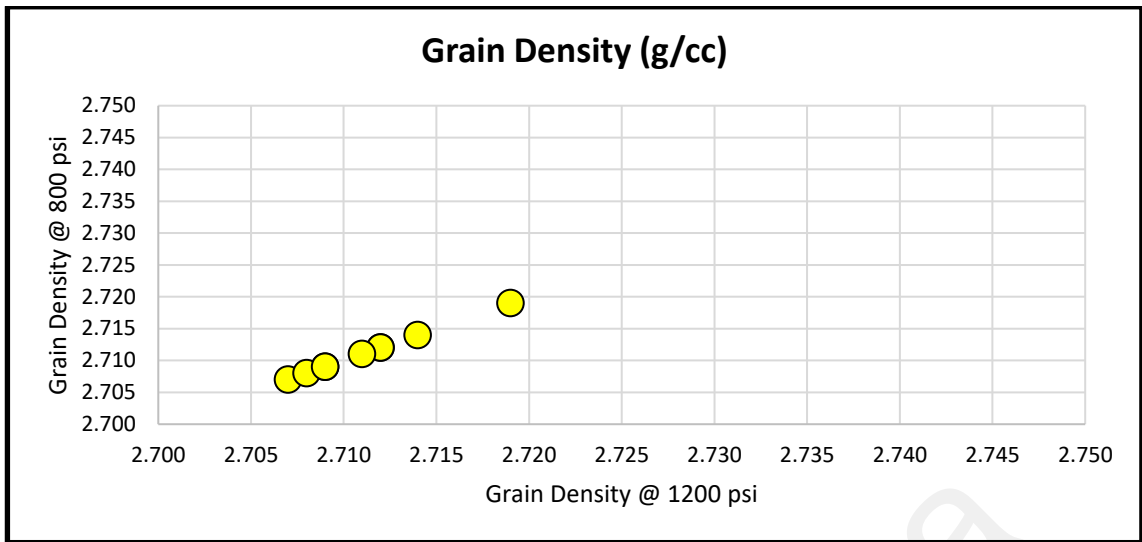
Figure 4.4: Grain density sensitivity plot.

Table 4.7 lists the permeability and porosity measurement the selected core plugs pre and post CO_2 injection. The grain density value of 2.71 g/cc was observed, which shows a typical number for limestone formation. Nitrogen was used as a conduit through a porosimeter and validated using the calculation in Equation 3.3.

Table 4.7: Comparison pre-post CO_2 injection (RCA).

Sample 1				
Sample Condition	Pre-CO_2 Injection	Post-CO_2 Injection	Pre-CO_2 Injection	Post-CO_2 Injection
Net Confining Stress (psi)	800		1200	
Kair (mD)	213	158	208	136
Kklinkenberg (mD)	172	104	158	87
Porosity (%)	26	25	26	25
Sample 2				
Sample Condition	Pre CO_2 Injection	Post-CO_2 Injection	Pre CO_2 Injection	Post-CO_2 Injection
Net Confining Stress (psi)	800		1200	
Kair (mD)	123	90	122	85
Kklinkenberg (mD)	81	50	78	60
Porosity (%)	29	27	29	27
Sample 3				
Sample Condition	Pre CO_2 Injection	Post-CO_2 Injection	Pre CO_2 Injection	Post-CO_2 Injection
Net Confining Stress (psi)	800		1200	
Kair (mD)	1824	1234	1744	1109
Kklinkenberg (mD)	1769	1005	1691	900
Porosity (%)	30	27	30	27

4.4   Brine and Effluent Analysis

Brine composition was formulated based on a brine sample from the B-3 field due to the unavailability of A water analysis. As mentioned previously, B and A field share common aquifer support; hence brine composition from this field was selected as a representative to be used as an analogy for A field. The brine sample was collected during production testing after the separator.

The water appearance was slightly cloudy prior to filtration and cleared afterward. Brine salinity reading for the B-3 field was 21223 ppm based on total NaCl constituent in the synthetic brine while the total dissolved solid was 22789 ppm. Table 4.8 and Table 4.9 represent effluent collected at each incremental flow rate used in this experiment pre and post CO_2 injection.

Table 4.8: Cation analysis of brine effluent pre and post-CO₂ injection.

Brine Effluent Post-CO₂ Injection Rate (ml/min)	Sodium, Na (mg/l)	Calcium, Ca (mg/l)	Magnesium, Mg (mg/l)	Potassium, K (mg/l)	Strontium (mg/l)	pH at 27 ℃
Sample 1						
Initial Brine	8748	0	0	3	0	8.5
4	8732	130	10	40	8	8.3
6	7236	146	13	61	12	8.3
8	5748	138	9	36	9	8.3
10	6916	330	13	64	12	8.4
12	8588	60	23	148	14	8.2
14	6275	467	30	107	15	8.2
16	6778	177	29	110	26	8.2
Sample 2						
Initial Brine	10230	0	28	111	22	6.4
4	10010	0	26	109	20	6.2
6	10220	0	27	116	21	6.3
8	10140	0	26	109	21	6.1
10	10340	0	28	115	21	6.3
12	10270	0	33	125	27	6.2
14	10400	0	28	116	25	6.3
16	10360	0	17	82	16	6.4

Sample 3						
Brine Effluent Post-CO₂ Injection Rate (ml/min)	**Sodium, Na (mg/l)**	**Calcium, Ca (mg/l)**	**Magnesium, Mg (mg/l)**	**Potassium, K (mg/l)**	**Strontium (mg/l)**	**pH at 27 °C**
Initial Brine	8824	149	33	85	378	8.0
4	8523	117	32	83	170	7.9
6	8301	147	32	87	118	7.8
8	8478	380	41	86	117	7.4
10	7649	462	43	80	92	7.7
12	7790	451	42	77	86	7.5
14	7677	433	36	78	82	7.4
16	8084	374	33	80	82	7.5

Table 4.9: Anion analysis of brine effluent post CO_2 injection.

Sample 1				
Brine Effluent Post CO₂ Injection Rate (ml/min)	**Sulphate, SO₄ (mg/l)**	**Chloride, Cl (mg/l)**	**Bicarbonate, HCO₃ (mg/l)**	**Carbonate, CO₃ (mg/l)**
Initial Brine	1080	12475	470	13
4	900	11790	1761	0
6	870	10371	965	0
8	660	8219	848	0
10	840	10224	939	0
12	900	12377	991	0
14	690	9589	1056	0
16	750	9833	1082	0

Table 4.9, continued.

Sample 2				
Brine Effluent Post CO₂ Injection Rate (ml/min)	**Sulphate, SO₄ (mg/l)**	**Chloride, Cl (mg/l)**	**Bicarbonate, HCO₃ (mg/l)**	**Carbonate, CO₃ (mg/l)**
Initial Brine	960	12155.8	1276	0
4	990	12475	1251	0
6	960	12915	2413	0
8	930	12573	1188	0
10	1020	13258	1238	0
12	990	13209	1113	0
14	960	13209	1238	0
16	990	13258	1276	0
Sample 3				
Brine Effluent Post CO₂ Injection Rate (ml/min)	**Sulphate, SO₄ (mg/l)**	**Chloride, Cl (mg/l)**	**Bicarbonate, HCO₃ (mg/l)**	**Carbonate, CO₃ (mg/l)**
Initial Brine	660	13404	470	0
4	450	12967	574	0
6	480	12967	574	0
8	360	13210	1409	0
10	360	12772	1422	0
12	330	12044	1266	0
14	360	12113	1317	0
16	360	13112	1082	0

Figure 4.5: Brine effluent post-CO₂ injection for sample 1.
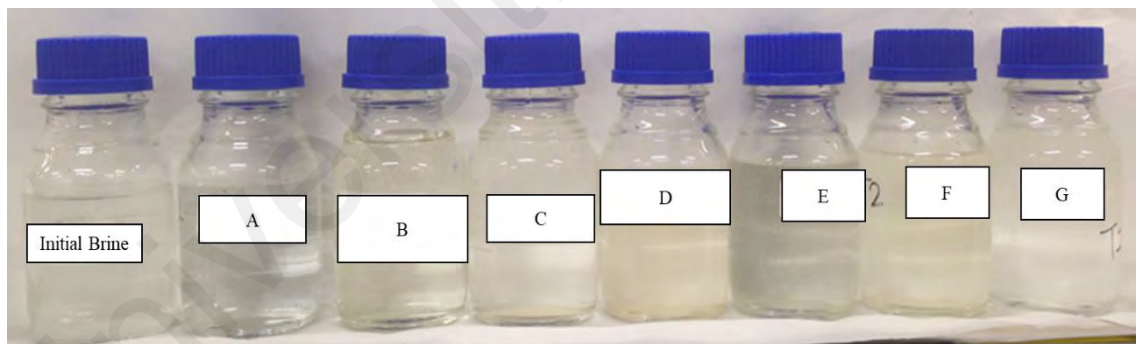
Figure 4.6: Brine effluent post-CO₂ injection at Q_{CO2} 4, 6, 8, 10, 12, 14 & 16 ml/min for bottle labels A, B, C, D, E, F, G respectively for sample 2.

Figure 4.5 and 4.6 indicates the occurrence of a cloudy solution for sample 1 and 2 post-CO₂ injection as an indication of geochemical reaction takes place between carbonate cores plugs and injected supercritical CO₂.

4.5 Multi-rate CO_2-Brine Injection Experiment

4.5.1 Reservoir Condition

Table 4.10 shows the values of the in-situ reservoir condition parameter used during experiments that were carried out under high temperature and high pressure. The pressure and temperature values used were the same as the in-situ reservoir conditions of the A field.

Table 4.10: In-situ reservoir condition.

Reservoir Pressure (psi)	Net Confining Stress (psi)	Temp (°C)	Seawater Gradient (psi/ft)	Overburden Pressure (psi)	Net Overburden Pressure – V (psi)	Overburden Pressure – H (psi)
3200	1564	140	0.443	5727	2527	1083

A preliminary study had been conducted, and the CO_2 will be injected at a depth of about 5556 ft from A seabed. Assumptions employed for this calculation are overburden gradient at one psi/ft and Poisson ratio equivalent to 0.3.

4.5.2 Water Permeability

A total of 3 sets of cyclic-coreflooding experiments were conducted during laboratory work, out of which all of them generated quality data to be presented here. The water permeability experiment was conducted prior to the major experiments to confirm the liability of the core plug for the analysis. In order to test this theory, an incremental water rate of 0.5, 1.0, and 1.5 ml/min were flowed at approximately 100 minutes or until it reaches stabilized differential pressure. Then, a decremented water rate of 1.5, 1.0, and 0.5 ml/min was injected to ensure the differential pressure at the incremental rate is equivalent to the decremented rate.

Figure 4.7, 4.8, and 4.9 indicate differential pressure versus time of selected core plugs. Based on these Figures, the core plugs were in good condition, and the brine will still be intact if the brine flowed below 1.5 ml/min. Therefore, as a baseline, the brine was flowed at 1 ml/min throughout the coreflooding experiments to maintain rock integrity. The brine flow rate of 0.5 ml/min was not chosen as a baseline since it will take a longer time to reach a stabilized flow rate as compare to brine flowed at 1 ml/min.
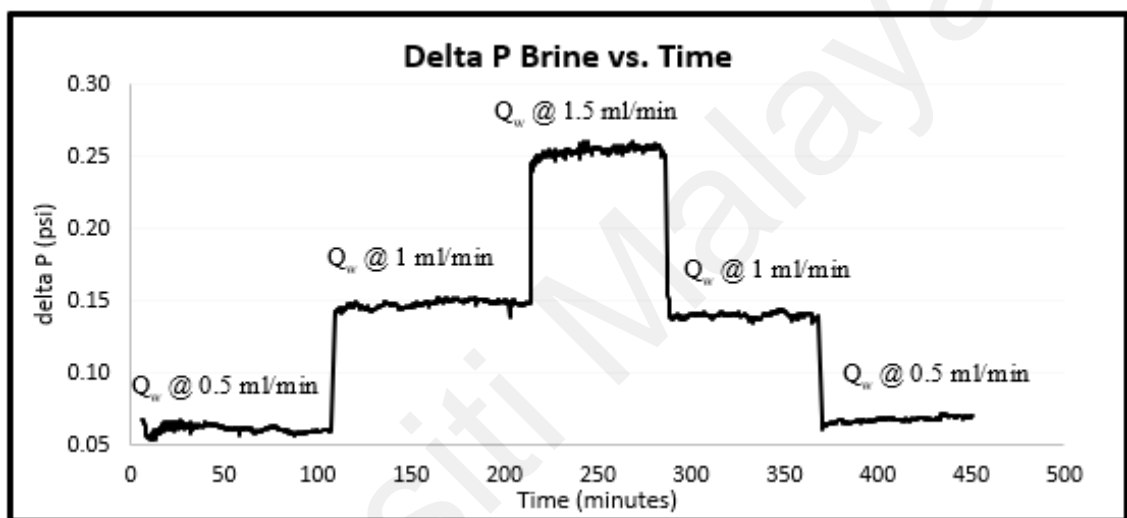

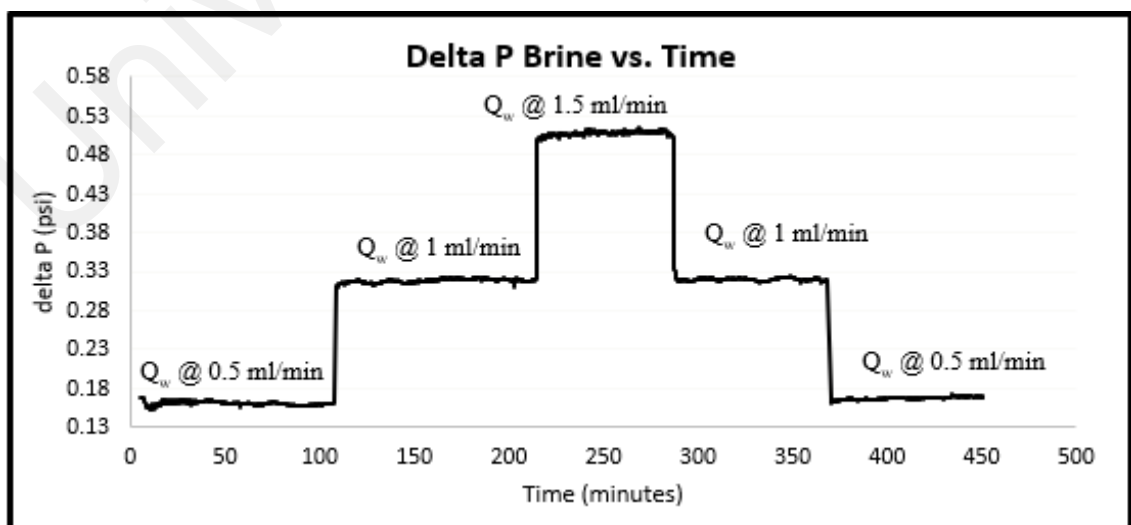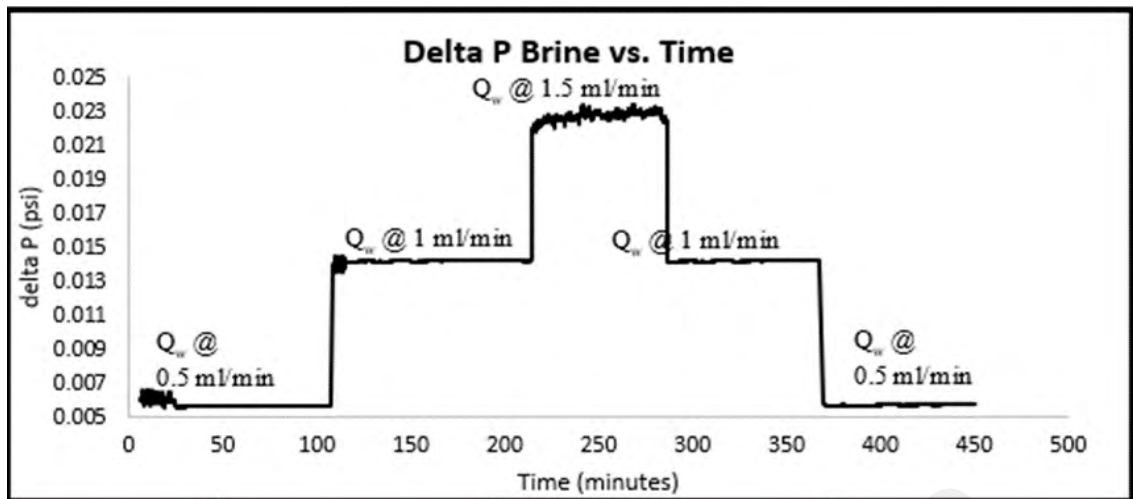**Figure 4.7: Delta P brine vs. time for sample 1; Kair = ~200 mD, ϕ = 26%.**

Figure 4.8: Delta P brine vs. time for sample 2; Kair = ~120 mD, ϕ = 29%.

Figure 4.9: Delta P brine vs. time for sample 3; Kair = ~1700 mD, φ = 30%.

Other than permeability obtained using porosimeter, the permeability of brine can be calculated during this laboratory work. In order to do this, the differential pressure at each stabilized flow rate of 0.5, 1.0, and 1.5 ml/min was plotted on a different graph of delta pressure versus brine flow rate.
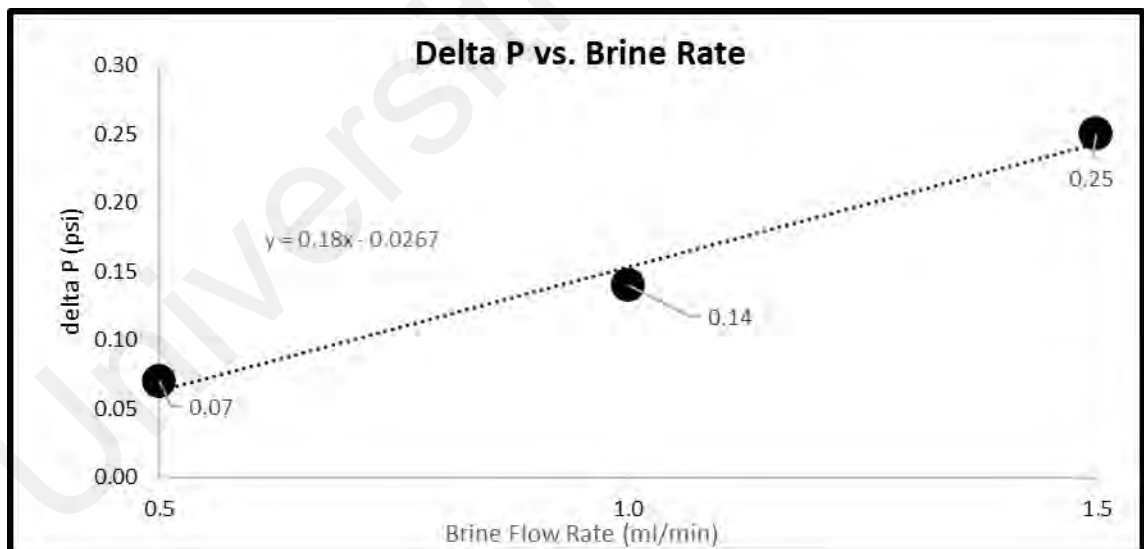
Figure 4.10: Delta P vs. brine rate for sample 1; Kair = ~200 mD, φ = 26%.

The slope of this graph is measured using the best-fit line, and the value was applied in the Darcy equation. Figures 4.10, 4.11, and 4.12 show differential pressure versus brine rate graphs, which eventually gives permeability value of 147, 76, and 1659 md.

These numbers are considered correct since these data are not far off from value obtained in Table 4.7 sample 2.
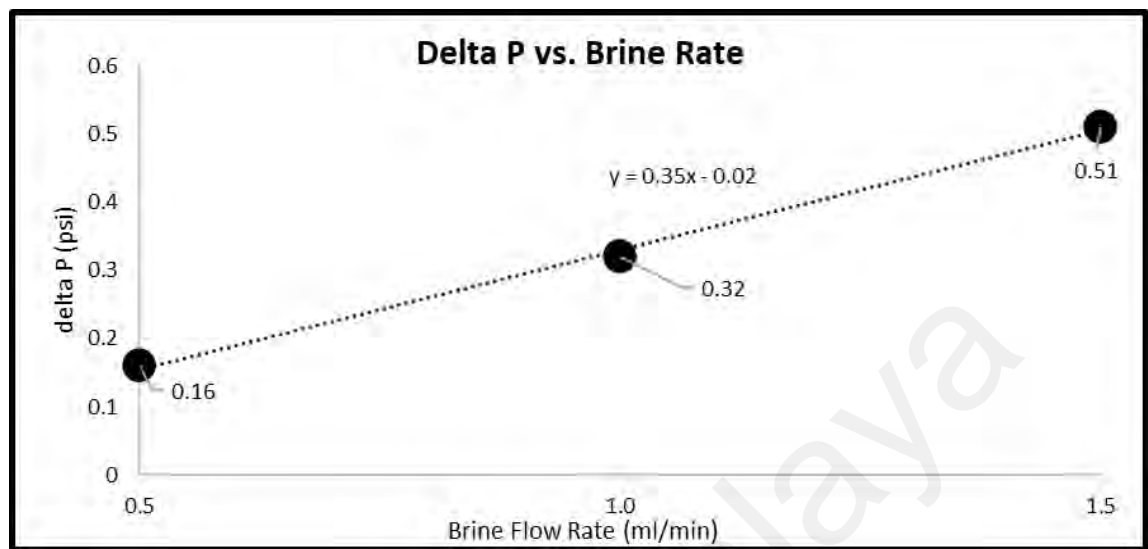
Figure 4.11: Delta P vs. brine rate for sample 2; Kair = ~120 mD, ϕ = 29%.
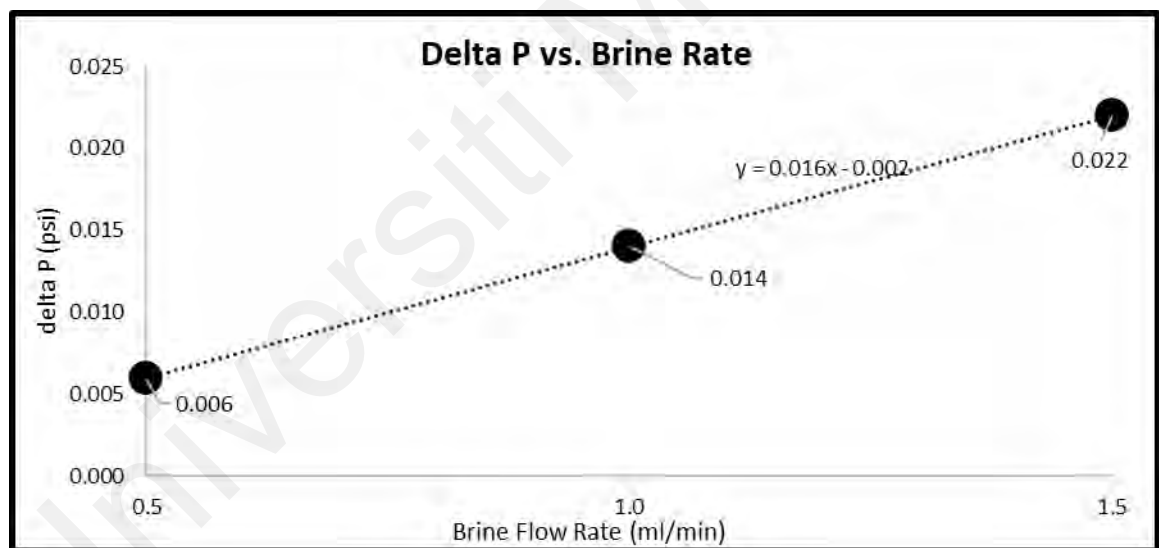
Figure 4.12: Delta P vs. brine rate for sample 3; Kair = ~1700 mD, ϕ = 30%.

It should be understood that the samples presented in this section were all carbonates and, with slight variations, all of conventional 1.500 (38.1 mm) diameter but with varying lengths. It is worth noting that the relationship between core plug permeability and the differential pressure between the inlet and outlet of the core is inverse proportional to each other.

4.5.3   Multi-rate CO₂ injection

Based on the CO_2 phase diagram, the requirement for CO_2 to be in the supercritical condition is to ensure the pressure and temperature of CO_2 must be above 1071 psi and 31°C, respectively. Supercritical CO_2 takes up much less space and diffuses better than in gas state through the tiny pore spaces in rocks, which lead to the higher CO_2 storage volume.

Figure 4.13 shows the alternate supercritical CO_2 and brine injection. The supercritical CO_2 was injected at incremental flow rate starting at 2 ml/min, 4 ml/min, 6 ml/min, 8 ml/min, 10 ml/min, 12 ml/min, and 16 ml/min.
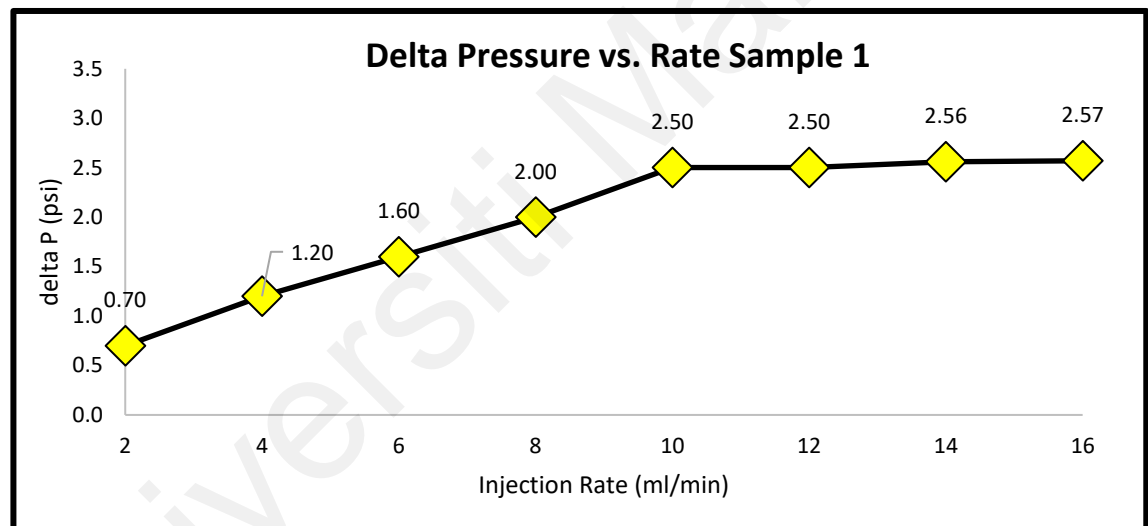
Figure 4.13: Delta P vs. sCO₂ injection rate for sample 1; Kair = ~200 mD, φ = 26%.

Brine was flowed at 1 ml/min after each incremental of CO_2 injection except after 16 ml/min of CO_2 injection prior to re-injection of CO_2 at 16 ml/min. At this point, the brine was injected at 1.5 ml/min. CO_2 was under supercritical condition at the point of injection.
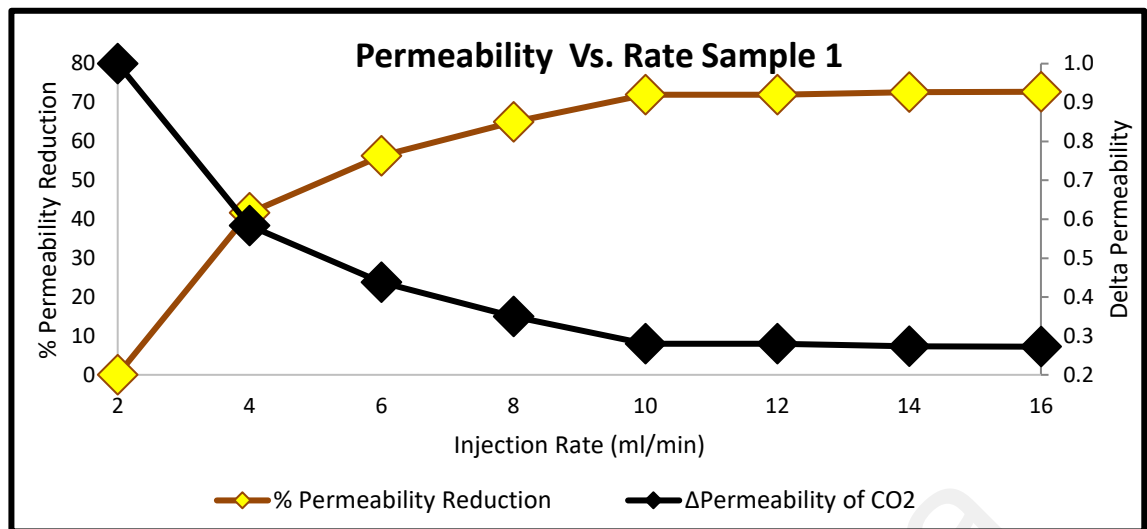
Figure 4.14: Permeability vs. sCO₂ injection rate for sample 1; Kair = ~200 mD, φ = 26%.

Brine injection was not captured in Figure 4.13 to simplify the graph and to make it easier for the reader to observe the CO_2 injection pattern. It must be understood that the rate presented in these graphs represent the supercritical CO_2 injection rate.

It seems that for Figure 4.13, the differential pressure trend line is increasing until, at a certain point that it reached a flattened curve. The point at which the curve started to have consistent differential pressure is considered as the critical rate. Therefore, it can be concluded that for sample 1, the critical rate is at 10 ml/min.

Observed in Figure 4.14 is the permeability versus rate for sample 1. The left axis is the percentage permeability reduction as the CO_2 flow inside the core plug at different injection rates. The permeability reduced significantly until it stopped at 80% of total core permeability, corresponding to the CO_2 critical rate.

Here again, the secondary axis plotted the difference between permeability reading at inlet and outlet due to the CO_2 production. As we can see from the graph, permeability goes lower as injection gets higher, and the curve flattened as it reaches a critical rate at 10 ml/min.
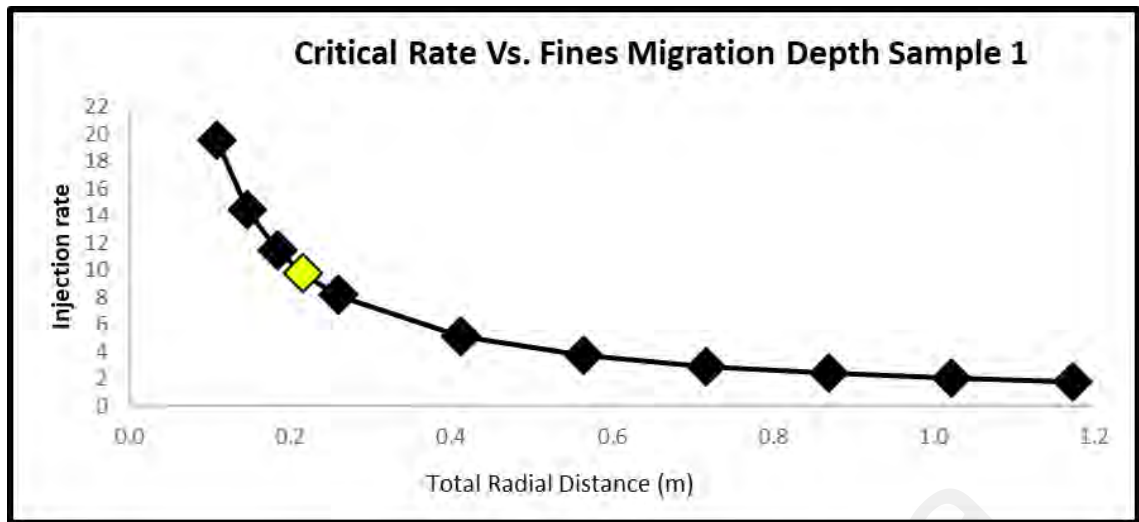
Figure 4.15: sCO₂ injection rate vs. Fines Migration Depth for sample 1; Kair = ~200 mD, ϕ = 26%.

The author also calculated the distance of the carbonate particle or debris could travel from the injection starting point, which can be seen in Figure 4.15. Meanwhile, Figure 4.16 illustrates the plotted data in Figure 4.15, 4.20, and 4.24. Sample 1 indicated that it could travel approximately up to 0.2 m from the injection point before it reaches a critical rate.
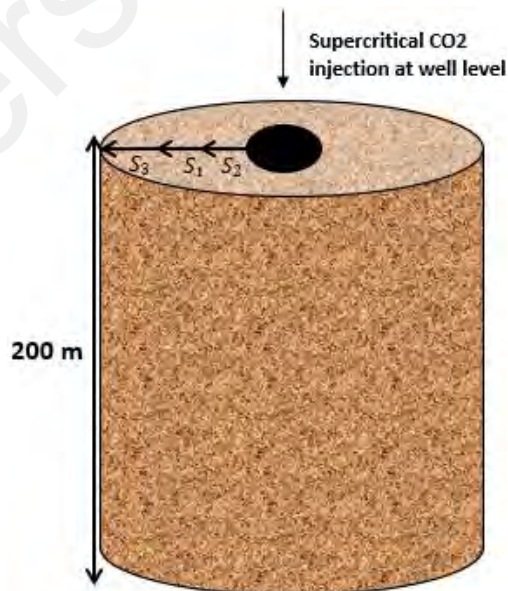
Figure 4.16: Illustration of sCO₂ at well level.

Figure 4.17 is the concentration ratio versus pore volume for sample 1. In this case, concentration for each injection rate was measured and plotted against the pore volume. It is worth noting that as the pore volume increases, the effluent concentration increases as more particles disperse or disintegrated from the core plug and experienced the geochemical reaction with the CO_2. The concentration ratio was calculated at the end of the pore volume with respect to the injection CO_2 rate.
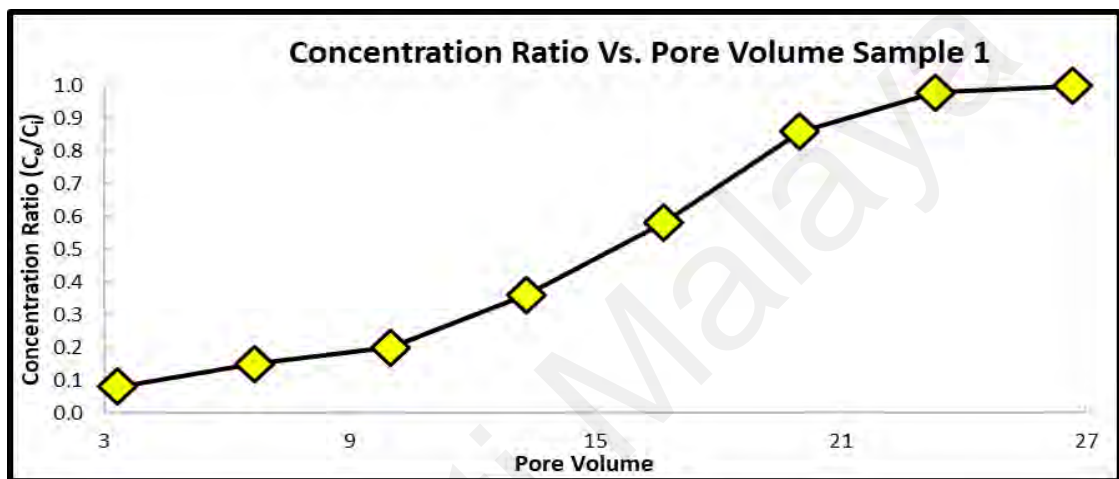
Figure 4.17: Concentration ratio vs. pore volume for sample 1; Kair = ~200 mD, ϕ = 26%.

Figure 4.18 represents delta pressure versus rate for sample 2. It should be noted that the same trend was observed, but sample 2 has reached the critical rate at 12 ml/min.
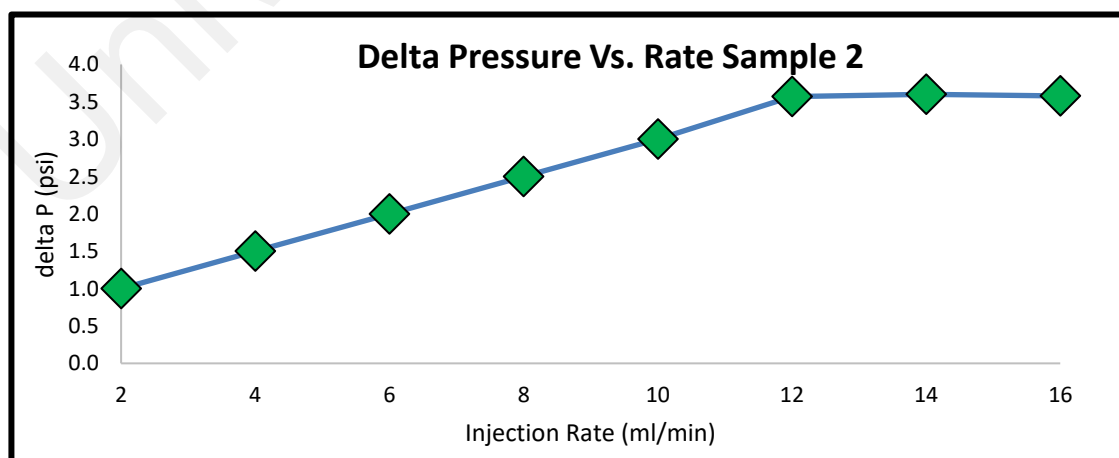
Figure 4.18: Delta P vs. sCO₂ injection rate for sample 2; Kair = ~120 mD, ϕ = 29%.

As can be seen in Figure 4.19, the permeability versus rate for sample 2 consists of percentage permeability reduction and delta permeability ration. Sample 2 has a maximum percentage permeability reduction at 70%, or in other words; the core permeability has destroyed up to 70 percent of its original condition.
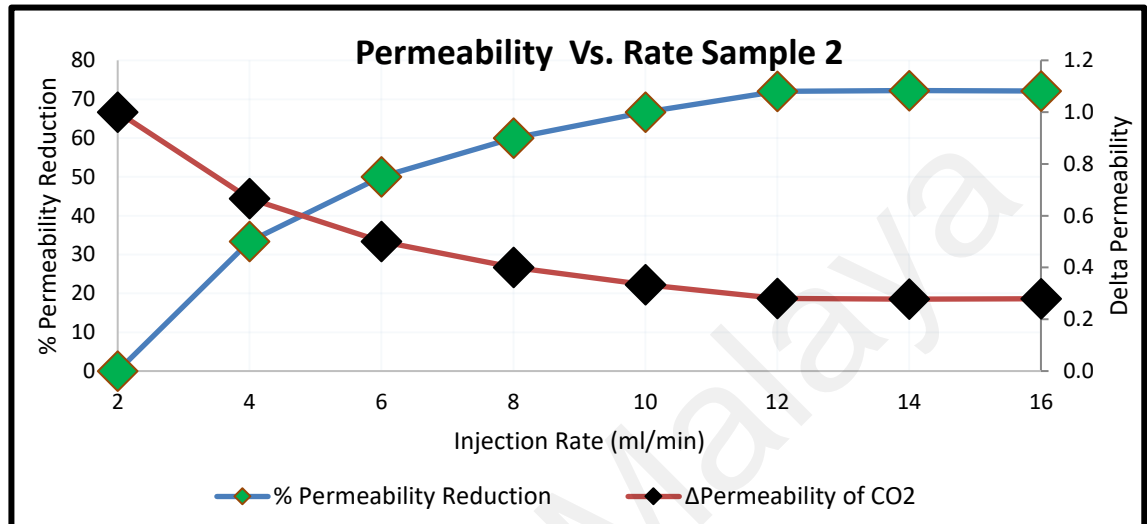
Figure 4.19: Permeability vs. sCO₂ injection rate for sample 2; Kair = ~120 mD, φ = 29%.

Sample 2 has the ability to travel up to around 0.19 m around the wellbore has it achieved a maximum injection rate at 12 ml/min, as shown in Figure 4.20.
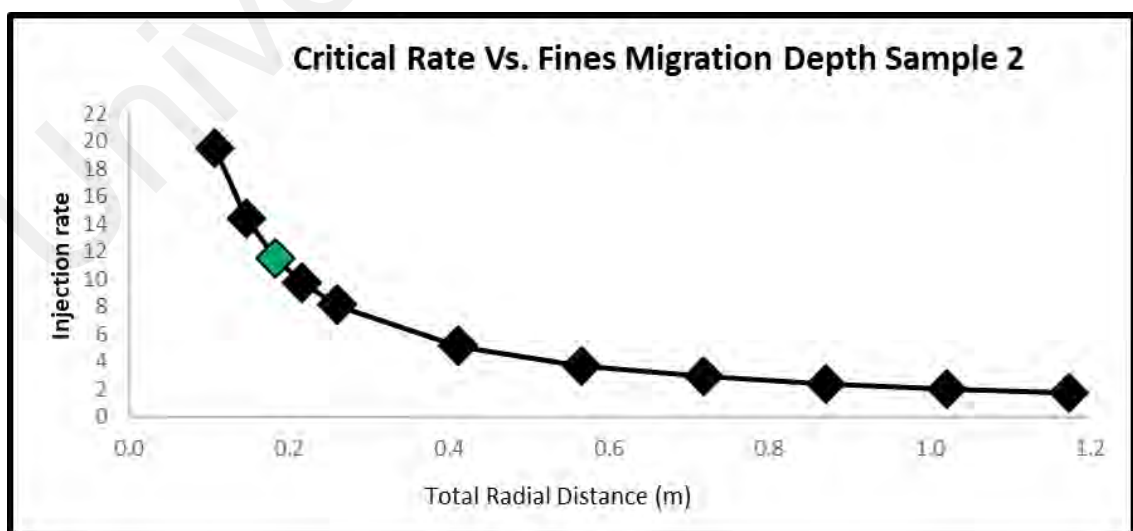
Figure 4.20: sCO₂ injection rate vs. Fines Migration Depth for sample 2; Kair = ~120 mD, φ = 29%.

The author has observed a similar trend for concentration versus pre volume data of sample 2 in Figure 4.21. The trend increases exponentially until it achieved a maximum concentration ratio.
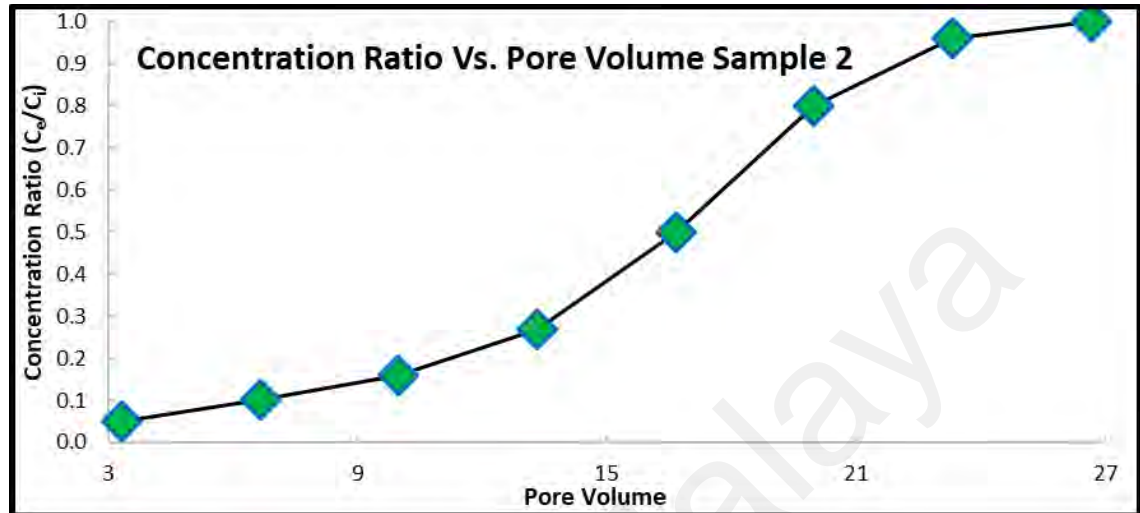
Figure 4.21: Concentration ratio vs. pore volume for sample 2; Kair = ~120 mD, φ = 29%.

Sample 3 differential pressure versus supercritical CO_2 injection rate plotted in Figure 4.22 showed that the sample had obtained the critical rate at 8 ml/min, and the graph flattened afterward.
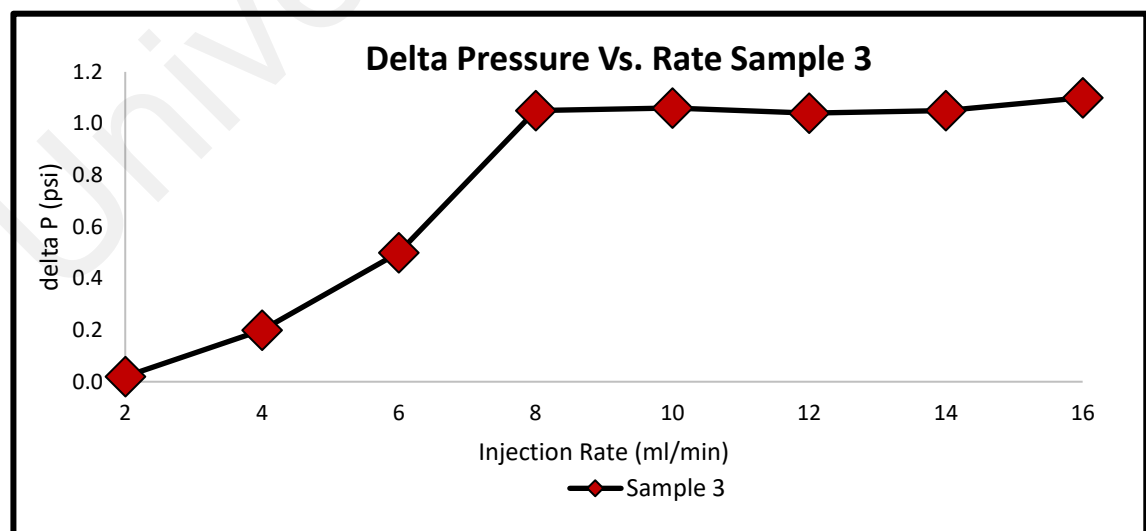
Figure 4.22: Delta P vs. sCO₂ injection rate for sample 3; Kair = ~1700 mD, φ = 30%.

Meanwhile, Figure 4.23 represents a significant incremental percentage permeability reduction at 4 ml/min as the CO_2 injected into the core plug.
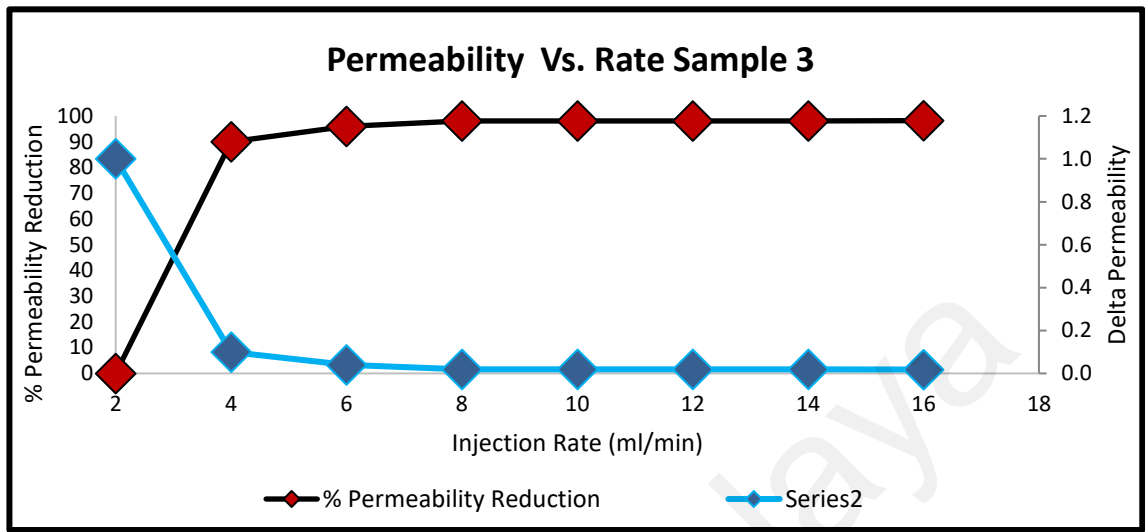
Figure 4.23: Permeability vs. sCO₂ injection rate for sample 3; Kair = ~1700 mD, ϕ = 30%.

In Figure 4.24, the graph indicated that the particles inside the core plug could travel approximately 0.22 m at field scale level from the injection point. The concentration ratio versus pore volume of sample 3 can be seen in Figure 4.25.
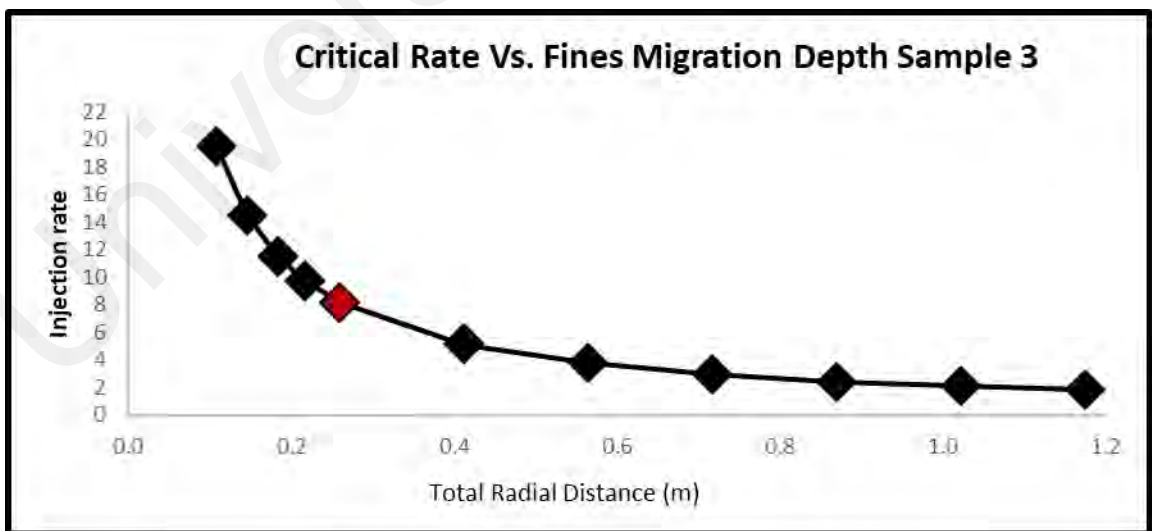
Figure 4.24: sCO₂ injection rate vs. Fines Migration Depth for sample 3;   Kair = ~1700mD, ϕ = 30%.
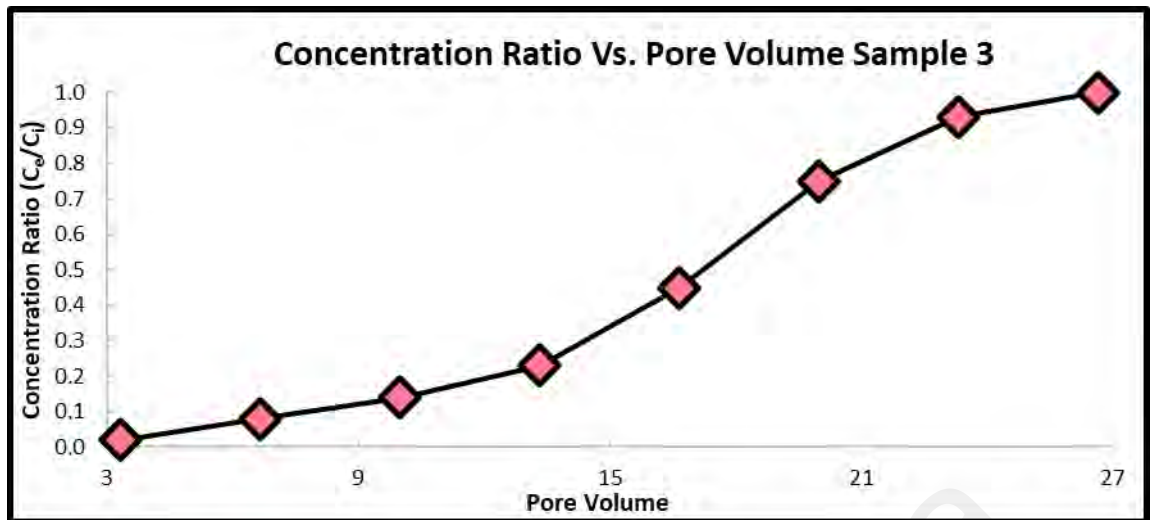
Figure 4.25: Concentration ratio vs. pore volume for sample 3; Kair = ~1700 mD, ϕ = 30%.

CHAPTER 5: DISCUSSION

5.1 Introduction

This chapter is dedicated to the interpretation, analyses, and discussion of results presented in Chapter 4. The effects of a number of factors on the multiphase flow characteristics of the rock-fluids system during underground CO_2 disposal will be critically analyzed and presented in this chapter. All laboratory works were designed to meet the common goal of the research objectives.

5.2 The critical rate of CO_2 injection

Presented in Figure 5.1 is the comparison study between three core plug samples of different permeability. The author would like to highlight that the water permeability of sample 1, sample 2, and sample 3 are approximately 147, 76, and 1659 mD, respectively. Therefore, the characteristic of these samples is different and observed based on the critical rate achieved during the experiments.
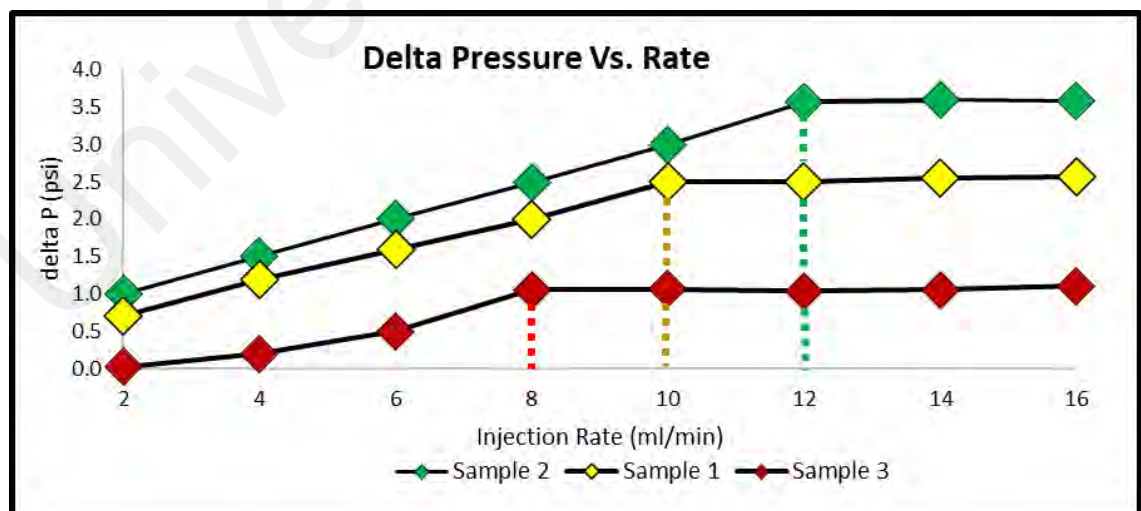
Figure 5.1: Delta P vs. sCO_2 injection rate; sample 1; Kair = ~200 mD, ɸ = 26%; sample 2; Kair = ~120 mD, ɸ = 29%; sample 3; Kair = ~1700 mD, ɸ = 30%.

Figure 5.1 shows the differential pressure inside the core plug against the supercritical CO_2 injection rate with Sample 2 that has lowest permeability exhibit the highest critical rate, followed by sample 1 and sample 3 in descending order. As CO_2 injection rate was getting higher, fines continue to migrate from core plugs causing the ΔP to continue to raise until the flow rate was unable to reach stabilized ΔP. Since the highest permeability core plug possess the lowest differential pressure, it will be easier for the core plug to reach its critical rate as it gets easier for the solid particle to disperse from the main body and build up at the core plug outlet. Meanwhile, for the lower permeability core plug, the integrity of the structure is firmer and stronger that makes it more difficult for these rocks to react with supercritical CO_2 and travel through the coreflood system.
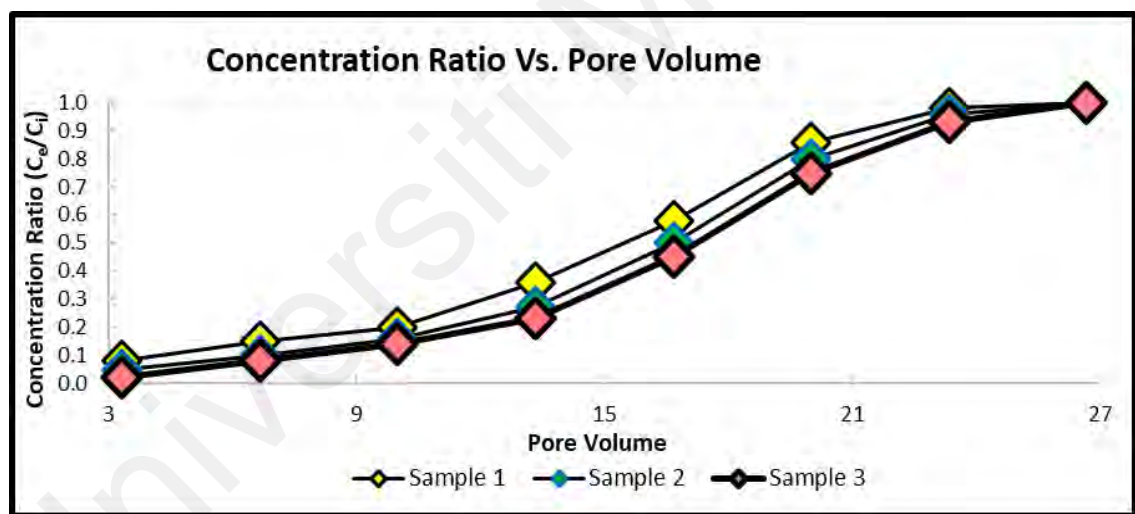
Figure 5.2: Concentration ratio vs. pore volume; sample 1; Kair = ~200 mD, ɸ = 26%; sample 2; Kair = ~120 mD, ɸ = 29%; sample 3; Kair = ~1700 mD, ɸ = 30%.

Plotted in Figure 5.2 is the resemblance pattern of concentration ratio versus pore volume for all three core plug samples. As previously mentioned, the highest permeability samples carry the lowest concentration ratio as compared to the lowest permeability core. To the best knowledge of the author, such experimental results as those presented here could be due to the fact that core plug sample 1 experienced the

greatest geochemical reaction as compared to sample 3 at the same pore volume measurement.
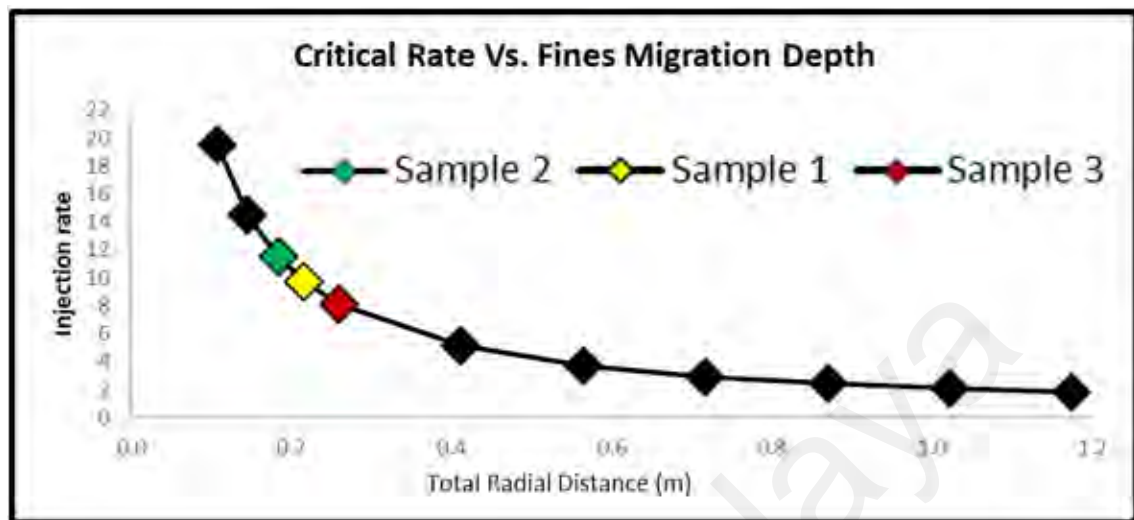
Figure 5.3: sCO$_2$ injection rate vs. Fines Migration Depth; sample 1; Kair = ~200 mD, ϕ = 26%; sample 2; Kair = ~120 mD, ϕ = 29%; sample 3; Kair = ~1700 mD, ϕ = 30%.

Despite the fact that there may not be a valid universal relationship defined between the injection rate and distance travel by the solid particles to block the pathway, experimental analyses through this research has confirmed that as critical rate gets higher, the chances at well level are the supercritical CO$_2$ will crack the formation at a shorter distance than that of lower critical rate CO$_2$ injection, as shown in Figure 5.3.

It can be deduced that based on three different native core plugs that were used in this experiment, solid particles of sample 3 that consist of the highest permeability of all core plugs have the ability to allow the crack happen further away for the wellbore.

To the best knowledge of the author, to date, the data presented in this thesis is the most comprehensive discussion on the critical rate analysis. In high permeability samples and samples susceptible to formation damage (e.g. fines migration, mineral dissolution/precipitation, etc.) the critical rate (represented during the experiments by the differential pressure across the samples) may decrease as the cyclic CO$_2$-brine

injection proceeds. However, it is predicted that the extent of any reduction in the injectivity would stabilize after several injection cycles.

The author concluded that for the formation that has permeability range between 100 to 1000 mD, the critical rate would be around 10 ml/min, in which the disperse particle could travel up to 0.19 m around the wellbore before the formation breaks. Meanwhile, for rock permeability of 1000 to 10000 mD, and 10 to 100 mD, the critical rate would be 8 ml/min and 12 ml/min, respectively, with the ability to travel up to around 0.2 and 0.22 m.

5.3   The Geochemical Effect of CO_2 Injection

Several other phenomena have encountered, such as scaling due to brine chemistry, mineral dissolution, and precipitation post-CO_2 injection. These chemical changes would have a significant impact on the determination of the critical rate. However, the rate of chemical reaction occurs at less speed compare to physical changes. That is the reason why the critical rate is observed for all samples.
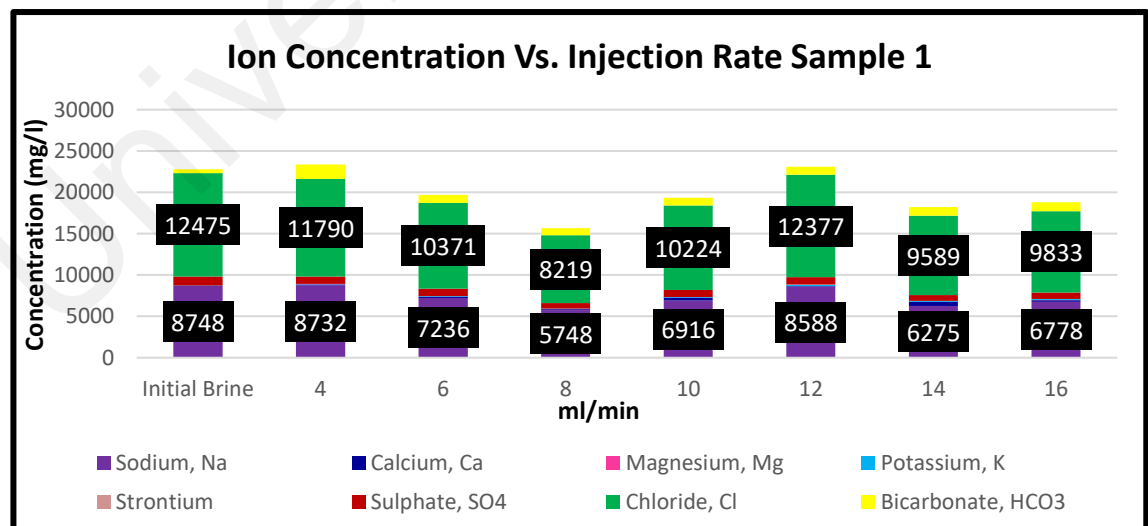
Figure 5.4: Ion concentration vs. injection rate for sample 1; Kair = ~200 mD, ϕ = 26%.

Continuous CO_2 WAG experiment must be conducted without stopping to avoid an increase in the chemical reaction between fluid-rock, which would result in a serious error during the interpretation of the lab experiments. It is necessary to point out that the data plotted in Figure 5.4 until 5.6 indicated that the precipitation occurs due to the dry-out phenomenon caused by the evaporation of NaCl if the reader observed reduction in sodium cation effluent collected after the CO_2 injection.
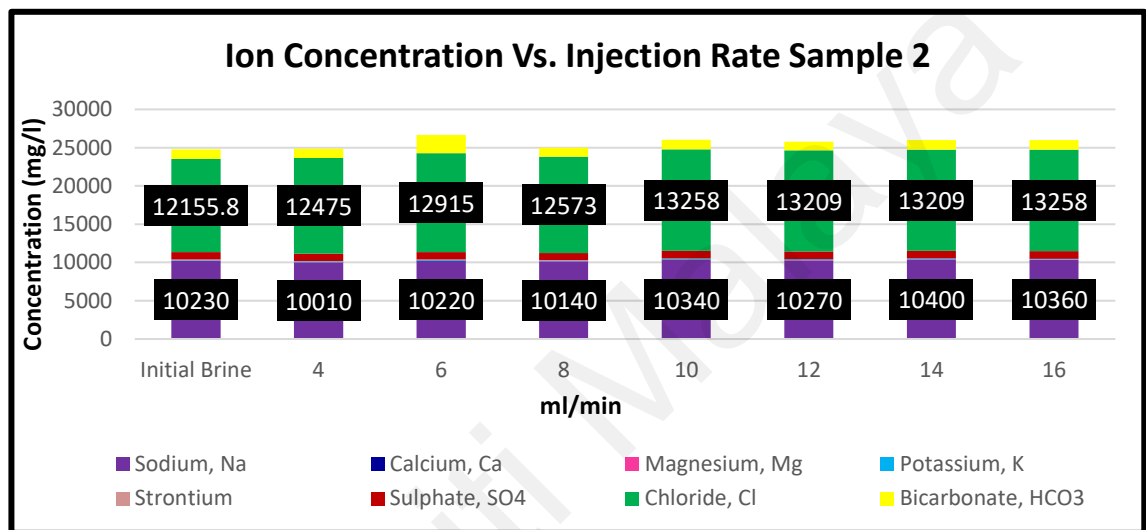

Figure 5.5: Ion concentration vs. injection rate for sample 2; Kair = ~120 mD, ϕ = 29%.
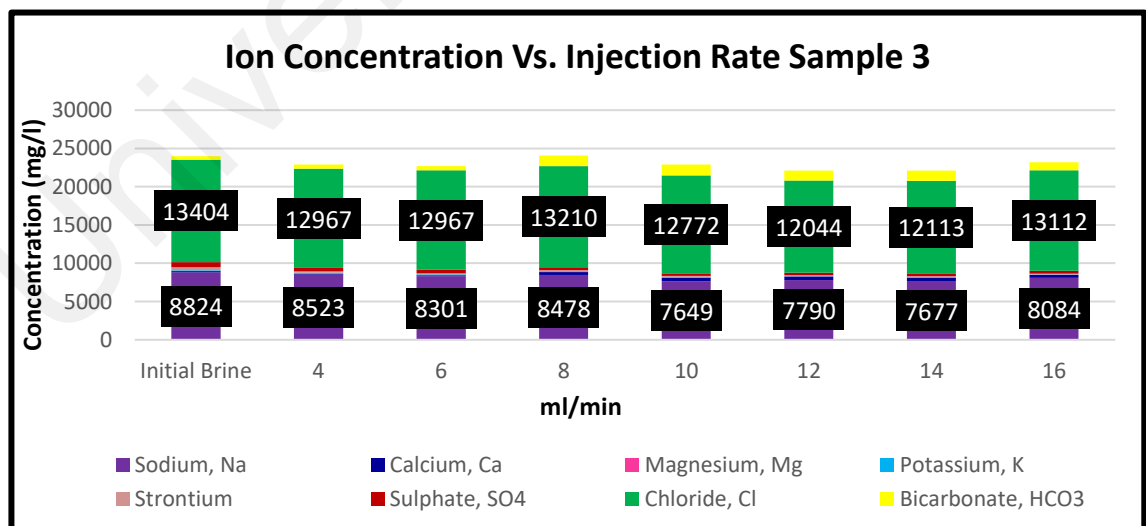
Figure 5.6: Ion concentration vs. injection rate for sample 3; Kair = ~1700 mD, ϕ = 30%.

These solid particles eventually blocked the pore throats and directly hindered any fluid movement inside the core plug. Reduction in ions indicates that precipitation takes place, while an increase in ions in the effluent represents the dissolution of minerals.

The limitations of this experiment in term of geochemical analysis are:

i.   The effluent was tested at an ambient condition that might not be representative of reservoir conditions.

ii. The pH reading during coreflooding experiment (reservoir condition) rather than after the back-pressure regulator (ambient condition).

iii. It is also recommended to utilize a bigger brine accumulator in order to cater to up to 300 pore volume of brine and/or CO_2 injection because the increase in reaction time between the core plug and brine would definitely impact the output data that is required for injectivity study.

5.4 CO_2-brine-rock Multiphase Flow Behavior Impact Permeability and Porosity

Figure 5.7 until 5.12 show a comparison between the permeability and porosity calculated for the three samples, pre and post CO_2 injection at 800 psia and 1200 psia net confining stress. Observation on the physical characteristic of core plugs can be concluded that the permeability and porosity of the core plug sample have been destroyed due to geochemical reactions occur between the physical core plug and the acidic solution, and physical reaction between the flow rates and the core plug. The porosity and permeability have reduced from its original value after exposed to supercritical CO_2 injection regardless of net confining stress.

Figure 5.7: Changes in permeability and porosity due to supercritical CO₂ injection at 800 psia net confining stress sample 1; Kair = ~200 mD, φ = 26%.

Figure 5.8: Changes in permeability and porosity due to supercritical CO₂ injection at 1200 psia net confining stress sample 1; Kair = ~200 mD, φ = 26%.
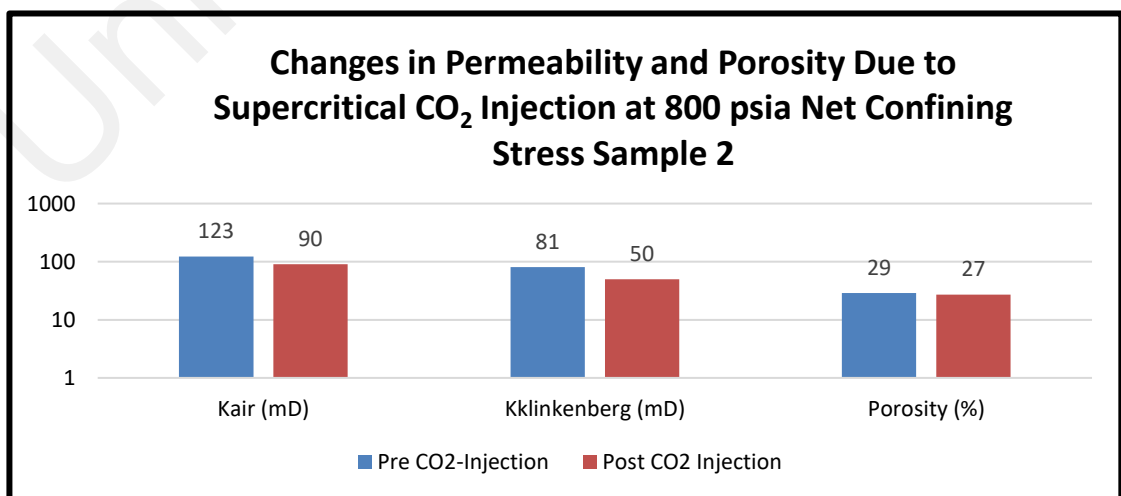
Figure 5.9: Changes in permeability and porosity due to supercritical CO₂ injection at 800 psia net confining stress sample 2; Kair = ~120 mD, φ = 29%.

Figure 5.10: Changes in permeability and porosity due to supercritical CO_2 injection at 1200 psia net confining stress sample 2; Kair = ~120 mD, ϕ = 29%.
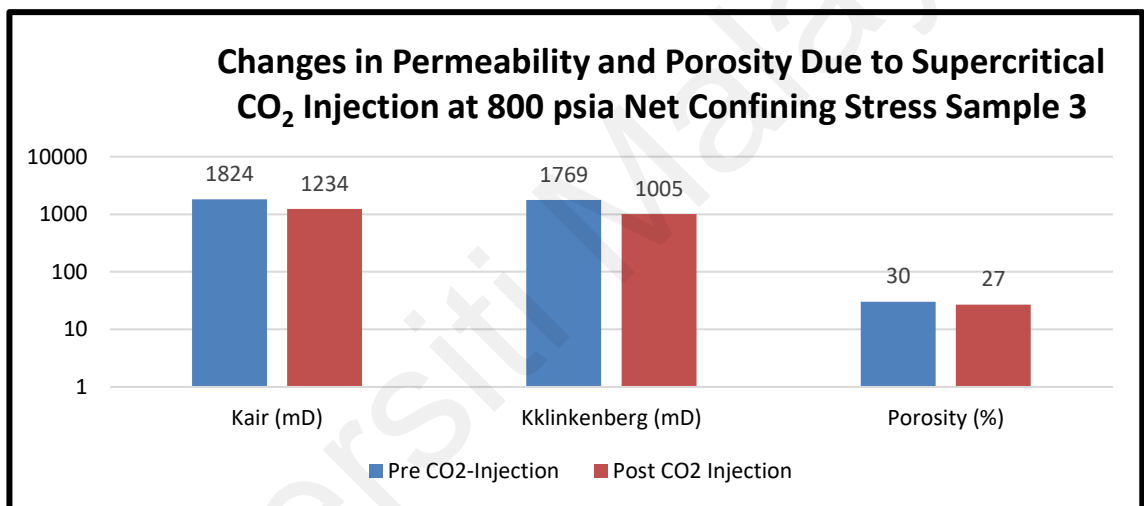
Figure 5.11: Changes in permeability and porosity due to supercritical CO_2 injection at 800 psia net confining stress sample 3; Kair = ~1700 mD, ϕ = 30%.
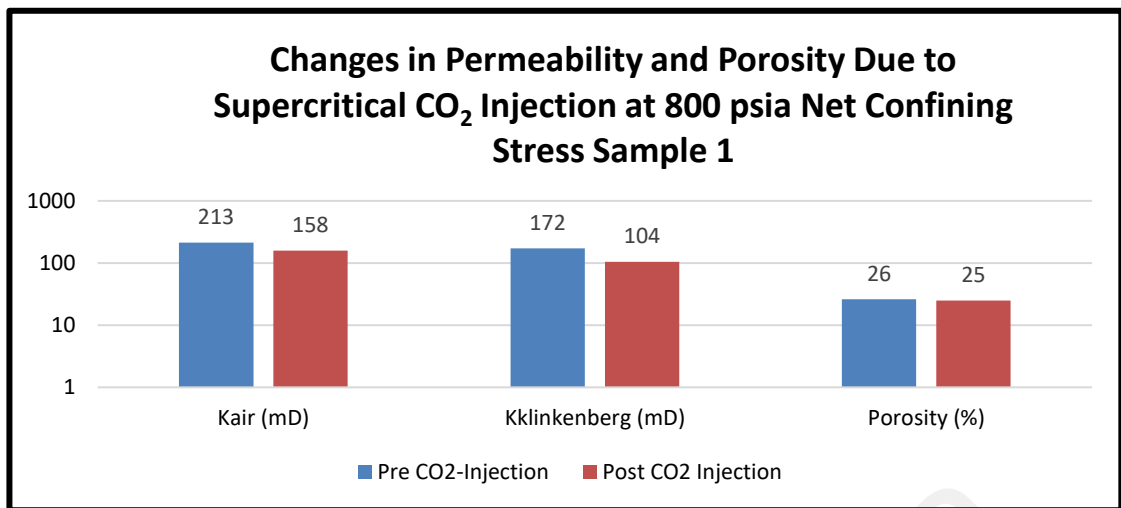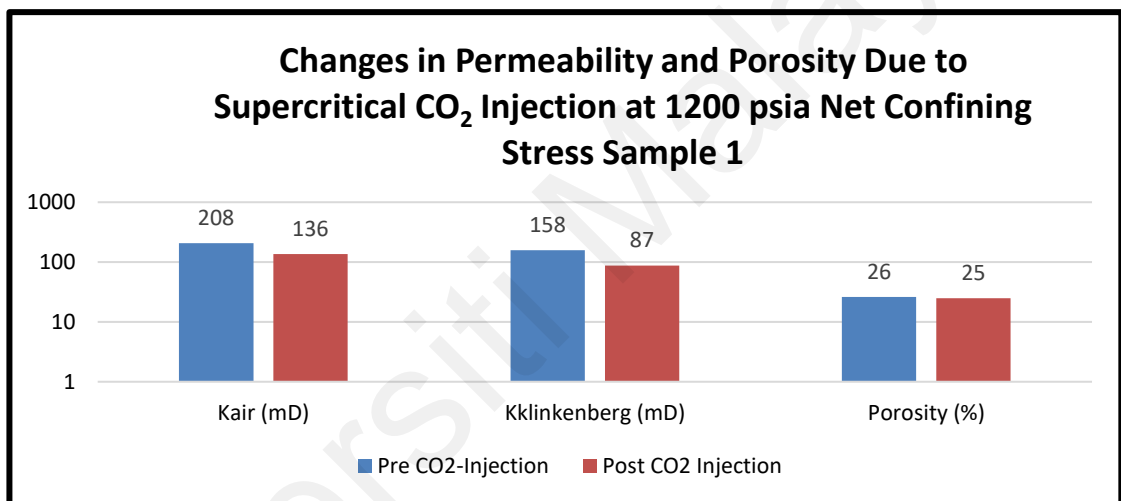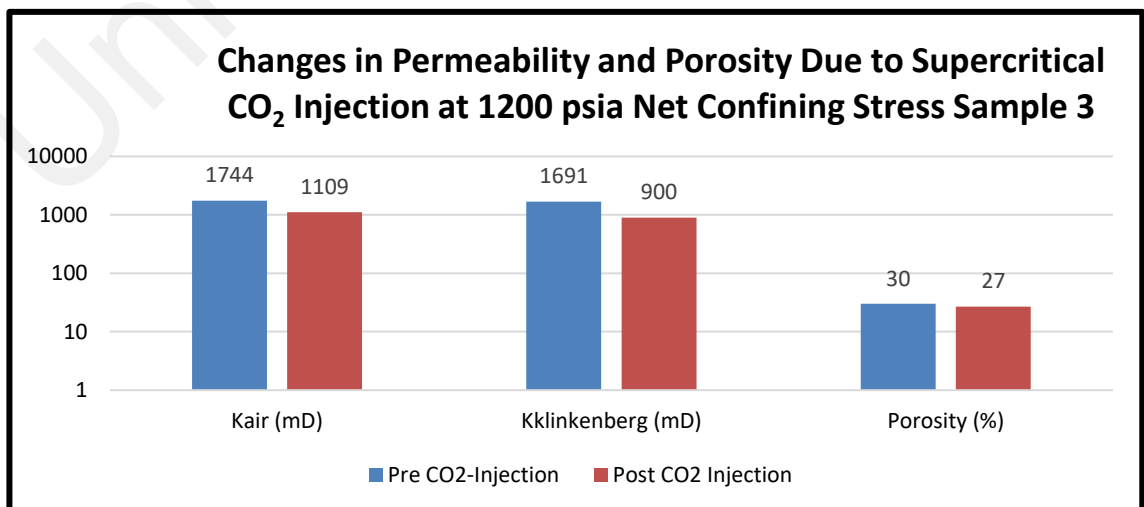

Figure 5.12: Changes in permeability and porosity due to supercritical CO_2 Injection at 1200 psia Net Confining Stress Sample 3; Kair = ~1700 mD, ϕ = 30%.
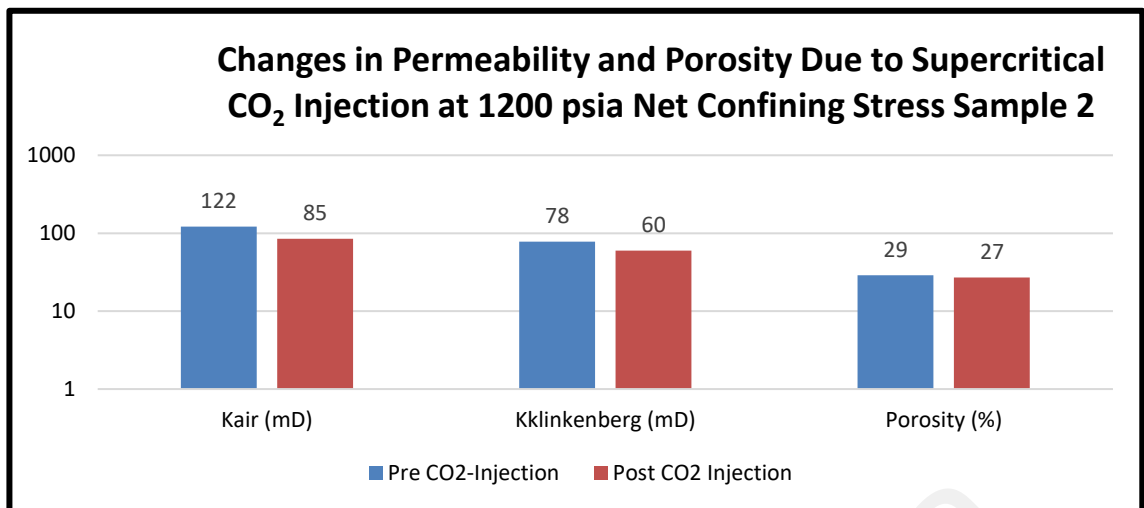
CHAPTER 6: CONCLUSION

In conclusion, the recent work on the CO_2 injection into a carbonate field using Malaysia limestone can be summarized as follows;

i.   The formation heterogeneity around the wellbore will not result in formation damage due to fines migration if CO_2 is injected within a safe injection limit. Injection below the critical limit by taken into account permeability rock is crucial to avoid formation damage around the wellbore. Nevertheless, looking at the geochemical perspective, if the injection rate is too slow, it will cause more chemical reactions between fluid and rock due to a longer time taken to for the CO_2 to flow within the core plug.

ii. Several other phenomena have encountered, such as scaling due to brine chemistry, mineral dissolution, and precipitation from post-CO_2 injection. These chemical changes would have a significant impact on the determination of the critical rate. However, the rate of chemical reaction occurs at less speed compare to physical changes. That is the reason why the critical is observed for all samples. There are other samples that are not representative of this report have shown that the chemical reaction could occur at a higher speed than physical changes of the core that make it difficult for the author to conclude the critical rate analysis. Having said that, the core plug will not be suitable for this study. The author also has observed that it is at utmost important to run the coreflood experiment in continuous order without stopping to avoid an increase in a chemical reaction between fluid-rock, which would result in a serious error during the interpretation of the lab data.

iii. The experimental approach presented here seems to quantitatively explain the features of solid particle transport and the critical rate observed in heterogenous Malaysian limestone. The experimental methodology might as well be used for prediction of critical rate for CO_2 sequestration in other areas.

It is recommended to have optimum tubing size and good material selection of tubing for highly corrosive CO_2. CO_2 plume migration surveillance and monitoring should be conducted throughout the field life to ensure the safety of CO_2 injection and storage. Oil and gas community should be looking into different aspect of CO_2 injection such as the existence of other impurity such as hydrogen sulphide.

REFERENCES

Akintunde, O. M., Knapp, C., & Knapp, J. (2013). Petrophysical characterization of the South Georgia Rift Basin for supercritical CO_2 storage: a preliminary assessment. *Environmental Earth Sciences, 70*(7), 2971-2985.

Bachu, S. (2003). Screening and ranking of sedimentary basins for sequestration of CO_2 in geological media in response to climate change. *Environmental Geology, 44*(3), 277-289.

Chu, S. (2009). Carbon capture and sequestration. *Science, 325*(5948), 1599.

Darcy, H. (1856). *Les fontaines publiques de la ville de Dijon: exposition et application.* Paris, France: Victor Dalmont.

Davison, J., Freund, P., & Smith, A. (2001). *Putting carbon back in the ground.* n.p.: IEA Greenhouse Gas R & D Programme.

Dunham, R. J. (1962). Classification of carbonate rocks according to depositional textures. *American Association of Petroleum Geologist Bulletin, Memoir 1*, 108-121.

Egermann, P., Bazin, B., & Vizika, O. (2005). *An experimental investigation of reaction-transport phenomena during CO_2 Injection*. Presented at the SPE Middle East Oil and Gas Show and Conference, 12-15 March 2005, Kingdom of Bahrain.

Emami-Meybodi, H., Hassanzadeh, H., Green, C. P., & Ennis-King, J. (2015). Convective dissolution of CO_2 in saline aquifers: Progress in modeling and experiments. *International Journal of Greenhouse Gas Control, 40*, 238-266.

Folk, R. L. (1959). Practical petrographic classification of limestones. *American Association of Petroleum Geologist Bulletin, 43*(1), 1-38.

Folk, R. L. (1962). Spectral subdivision of limestone types. *American Association of Petroleum Geologist Bulletin, Memoir 1,* 62-84.

Gant, P. L., & Anderson, W. G. (1988). Core cleaning for restoration of native wettability. *SPE formation evaluation, 3*(1), 131-138.

Global, C. (2015). The Global Status of CCS: 2015, Summary Report. Melbourne, Australia. Retrieved on 30 July 2020 from https://www.globalccsinstitute.com/wp-content/uploads/2018/12/Global-Status-Report_2015_Summary.pdf

Herzog, H. J. (2001). Peer reviewed: what future for carbon capture and sequestration?. *Environmental Science & Technology, 35*(7), 148-153.

Jalil, M. A. A., Masoudi, R., Darman, N. B., & Othman, M. (2012). *Study of the CO_2 injection, storage, and sequestration in depleted M4 carbonate gas condensate reservoir, Malaysia*. Presented at the Carbon Management Technology Conference, 7-9 February 2012, Orlando, Florida.

Jalil, M. A. A., Masoudi, R., Darman, N. B., Sofia, N. Z., & Othman, M. (2011). *Challenges in improving the hydrocarbon gas recovery: Case study using a carbonate gas condensate field in Malaysia*. Presented at the SPE Asia Pacific Oil and Gas Conference and Exhibition, 20-22 September 2011, Jakarta, Indonesia.

Jeddizahed, J., & Rostami, B. (2016). Experimental investigation of injectivity alteration due to salt precipitation during CO_2 sequestration in saline aquifers. *Advances in Water Resources, 96*, 23-33.

Jin, M., Ribeiro, A., Mackay, E., Guimarães, L., & Bagudu, U. (2016). Geochemical modelling of formation damage risk during CO_2 injection in saline aquifers. *Journal of Natural Gas Science and Engineering, 35*, 703-719.

Juanes, R., Spiteri, E., Orr, F., & Blunt, M. (2006). Impact of relative permeability hysteresis on geological CO_2 storage. *Water Resources Research, 42*(12).

Khanifar, A., Raub, M. R. A., Tewari, R. D., Zain, Z. M., & Sedaralit, M. F. (2015, Dec). *Designing of successful immiscible water alternating gas (IWAG) coreflood experiment*. Presented in the International Petroleum Technology Conference, 6-9 December 2015, Doha, Qatar.

Kok, K. H., Pruimboom, J., David, F. M., & Then, J. C. (2003). *Geosteer with resistivity forward modeling to prevent drilling into the loss circulation zone of a prolific carbonate reservoir*. Presented at the SPE/IADC Middle East Drilling Technology Conference and Exhibition, 20-22 October 2003, Abu Dhabi, United Arab Emirates.

Krumhansl, J., Pawar, R., Grigg, R., Westrich, H., Warpinski, N., Zhang, D., . . . Byrer, C. (2002, April). *Geological sequestration of carbon dioxide in a depleted Oil reservoir*. Presented at the SPE/DOE Improved Oil Recovery Symposium, 13-17 April 2002, Tulsa, Oklahoma.

Liu, F., Ellett, K., Xiao, Y., & Rupp, J. A. (2013). Assessing the feasibility of CO_2 storage in the New Albany Shale (Devonian–Mississippian) with potential enhanced gas recovery using reservoir simulation. *International Journal of Greenhouse Gas Control, 17*, 111-126.

Masoudi, R., Abd Jalil, M. A., Tan, C. P., Press, D., Keller, J., Anis, L., . . . Othman, M. (2013). *Simulation of chemical interaction of injected CO_2 and carbonic acid based on laboratory tests in 3D coupled geomechanical modelling*. Presented in the the International Petroleum Technology Conference, 26-28 March 2013, Beijing, China.

Masoudi, R., Jalil, M. A. A., Press, D. J., Lee, K.-H., Phuat Tan, C., Anis, L., . . . Othman, M. (2012). *An integrated reservoir simulation-geomechanical study on feasibility of CO_2 storage in M4 carbonate reservoir, Malaysia*. Presented in the the International Petroleum Technology Conference, 15-17 November 2011, Bangkok, Thailand.

Miranda, R. M., & Underdown, D. R. (1993). *Laboratory measurement of critical rate: A novel approach for quantifying fines migration problems*. Presented at the SPE Production Operations Symposium, 21-23 March, Oklahoma City, Oklahoma.

Miri, R., van Noort, R., Aagaard, P., & Hellevang, H. (2015). New insights on the physics of salt precipitation during injection of CO_2 into saline aquifers. *International Journal of Greenhouse Gas Control, 43*, 10-21.

Mohamed, I., & Nasr-El-Din, H. A. (2013). Fluid/rock interactions during CO_2 sequestration in deep saline carbonate aquifers: laboratory and modeling studies. *SPE Journal, 18*(03), 468-485.

Mohamed, I. M., He, J., & Nasr-El-Din, H. A. (2011). *Permeability change during CO_2 injection in carbonate aquifers: Experimental study*. Presented at the SPE Americas E&P Health, Safety, Security, and Environmental Conference, 21-23 March 2011, Houston, Texas.

Mora, C., Frazier, A. G., Longman, R. J., Dacks, R. S., Walton, M. M., Tong, E. J., . . . Giambelluca, T. W. (2013). The projected timing of climate departure from recent variability. *Nature, 502*(7470), 183-187.

Muller, N., Qi, R., Mackie, E., Pruess, K., & Blunt, M. J. (2009). CO_2 injection impairment due to halite precipitation. *Energy Procedia, 1*(1), 3507-3514.

Nasr-El-Din, H., Lynn, J., & Al-Dossary, K. (2002). *Formation damage caused by a water blockage chemical: prevention through operator supported test programs*. Paper presented in the International Symposium and Exhibition on Formation Damage Control, 20-21 February 2002, Lafayette, Louisiana.

Nguyen, P. T., Zeinijahromi, A., & Bedrikovetsky, P. G. (2012). *Taking advantage of fines migration formation damage for enhanced gas recovery*. Paper presented at the SPE International Symposium and Exhibition on Formation Damage Control, Lafayette, Louisiana, USA.

Ott, H., Roels, S. M., & de Kloe, K. (2015). Salt precipitation due to supercritical gas injection: I. Capillary-driven flow in unimodal sandstone. *International Journal of Greenhouse Gas Control, 43*, 247-255.

Pachauri, R. K., Allen, M. R., Barros, V. R., Broome, J., Cramer, W., Christ, R., . . . Dasgupta, P. (2014). *Climate change 2014: Synthesis report. Contribution of working groups I, II and III to the fifth assessment report of the Intergovernmental Panel on Climate Change* (pp. 151). Geneva, Switzerland: IPCC.

Pentland, C. H., El-Maghraby, R., Georgiadis, A., Iglauer, S., & Blunt, M. J. (2011). Immiscible displacements and capillary trapping in CO_2 storage. *Energy Procedia, 4*, 4969-4976.

Pham, H. S., Alpy, N., Mensah, S., Tothill, M., Ferrasse, J. H., Boutin, O., . . . Saez, M. (2016). A numerical study of cavitation and bubble dynamics in liquid CO_2 near the critical point. *International Journal of Heat and Mass Transfer, 102*, 174-185.

Polak, S., Cinar, Y., Holt, T., & Torsæter, O. (2011). An experimental investigation of the balance between capillary, viscous, and gravitational forces during CO_2 injection into saline aquifers. *Energy Procedia, 4*, 4395-4402.

RP40, A. (1960). *API recommended practice for core-analysis procedure*. New York, US: API.

Rubin, E. (2005). Technical Summary. In B. Metz, O. Davidson, H. D. Coninck, M. Loos & L. Meyer (Eds.), *IPCC Special Report on Carbon Dioxide Capture and Storage* (pp. 17). New York, US: Cambridge University Press.

Rushing, J., Newsham, K., Lasswell, P., Cox, J., & Blasingame, T. (2004). *Klinkenerg-corrected permeability measurements in tight gas sands: steady-state versus unsteady-state techniques*. Presented at the SPE Annual Technical Conference And Exhibition, 26-29 September 2004, Houston, Texas.

Saeedi, A. (2012). Experimental setup, material and procedure. In A. Saeedi (Ed), *Experimental study of multiphase flow in porous media during CO_2 Geo-sequestration processes* (pp. 51-89): Berlin, Germany: Springer-Verlag.

Saeedi, A., & Rezaee, R. (2012). Effect of residual natural gas saturation on multiphase flow behaviour during CO_2 geo-sequestration in depleted natural gas reservoirs. *Journal of Petroleum Science and Engineering, 82-83*, 17-26.

Scholle, P. A., & Ulmer-Scholle, D. S. (Eds.). (2003). *A color guide to the petrography of carbonate rocks: Grains, textures, porosity, diagenesis, AAPG Memoir 77* (Vol. 77). Tulsa, Oklahoma: AAPG.

Song, J., & Zhang, D. (2013). Comprehensive review of caprock-sealing mechanisms for geologic carbon sequestration. *Environ Science Technology, 47*(1), 9-22.

Tariq Janj, H., Mohammad A, A., & Parsed Gho, D. (2017). Sedimentology and reservoir geometry of the Miocene carbonate deposits in Central Luconia, Offshore, Sarawak, Malaysia. *Journal of Applied Sciences, 17*(4), 153-170.

Wang, J., Sun, B., Li, H., Wang, X., Wang, Z., & Sun, X. (2018). Phase state control model of supercritical CO_2 fracturing by temperature control. *International Journal of Heat and Mass Transfer, 118*, 1012-1021.

Wojtanowicz, A. K., Krilov, Z., & Langlinais, J. P. (1987). *Study on the effect of pore blocking mechanisms on formation damage*. Presented at the SPE Production Operations Symposium, 8-10 March 1987, Oklahoma City, Oklahoma.

Xu, T., Apps, J. A., & Pruess, K. (2005). Mineral sequestration of carbon dioxide in a sandstone–shale system. *Chemical Geology, 217*(3-4), 295-318.

Zhang, D., & Song, J. (2014). Mechanisms for geological carbon sequestration. *Procedia IUTAM, 10*, 319-327.